18

Ages and Interiors: the Cratering Record of the Galilean Satellites

Paul M. Schenk
Lunar and Planetary Institute

Clark R. Chapman
Southwest Research Institute

Kevin Zahnle, Jeffrey M. Moore
NASA Ames Research Center

18.1 INTRODUCTION

Impact craters on the Galilean satellites record not only the ages of their surfaces (in both absolute and relative terms), but also differences and changes in internal properties and thermal histories. The cratering record of the Galilean satellites is complex and success in unraveling these histories depends on having a complete morphologic and distributional description of the cratering record. The cratering record on these satellites is muddled by degradative processes that are not evident on rocky planets such as the Moon (see Chapter 17), although Mars has crater obscuration and degradation problems of its own. All evidence indicates that even the largest craters on Europa, Ganymede, and Callisto formed in an icy crust (Io's crust is dominated by silicates, see Chapter 14). This icy bedrock is potentially unstable, and some impact craters may relax or fade away to unrecognition due to water ice's volatility and weak but strongly temperature dependent rheology. The very properties of water ice that make craters susceptible to degradation also make them uniquely sensitive indicators of thermal histories and lithospheric states. Equally important, all the Galilean satellites act as witness plates for the bombardment history of the jovian system, despite the divergent geologic histories of each resulting in differing degrees of crater preservation.

It is important to recognize that the cratering records of all four satellites are entwined and must be examined *in toto*, and *in comparito*. In this chapter, we first examine how differences and changes in impact crater morphology and structure may record differences and changes in internal properties and possibly thermal state among the satellites. In some cases, impact crater deposits can be also used to deduce stratigraphic relationships, reveal the type of impactor, and determine the true sizes of large impact features with little remaining relief (e.g., palimpsests) in order to completely characterize the size–frequency distribution of large craters. We then examine the revised size–frequency distribution of impact craters on all the Galilean satellites to assess where impactors came from and the models that have been proposed to constrain how old these surfaces are. Of special interest are the tortured surface of Europa (Chapter 15) and the resurfaced bright terrains of Ganymede (Chapter 16). We also examine the distribution of craters and the potential effect of satellite rotation history on these records.

18.2 MORPHOLOGY

Nowhere in the solar system are impact morphologies observed in greater variety than on the large icy Galilean satellites Ganymede and Callisto (Figure 18.1). The first post-*Voyager* systematic study of these structures was that of Passey and Shoemaker (1982). Among other things, they concluded that most craters were flattened to lesser or greater degrees by flow (viscous relaxation) of the lithosphere as an expression of isostatic adjustment. The last comprehensive reviews of the state of impact crater lore on the jovian satellites were by Chapman and McKinnon (1986) and McKinnon *et al.* (1991). They also included a thorough review of impact mechanics in ice (although an update on mechanics is warranted, it is beyond our purview to do so here). More recent studies have focused on particular aspects of the cratering record, leading to the development of alternative hypotheses for the formation and evolution of specific crater types (e.g., Croft 1983, Thomas and Squyres 1990).

Several critical advances followed in the 1990s. Chief among these are new and reliable measurements of the topography and dimensions of impact crater structures and ejecta deposits (Schenk 1991, 1993, 2002, Schenk and Ridolfi 2002), which allow for detailed intersatellite comparison and correlation of morphologic differences. Ejecta deposits in particular are important because they can be used as a dimensional scaling tool in cases such as palimpsests where crater rims are no longer recognizable (Schenk and Ridolfi 2002). Secondly, *Galileo* has revealed the surprising europan crater morphology story where crater morphologies differ from those on Ganymede and Callisto (Moore

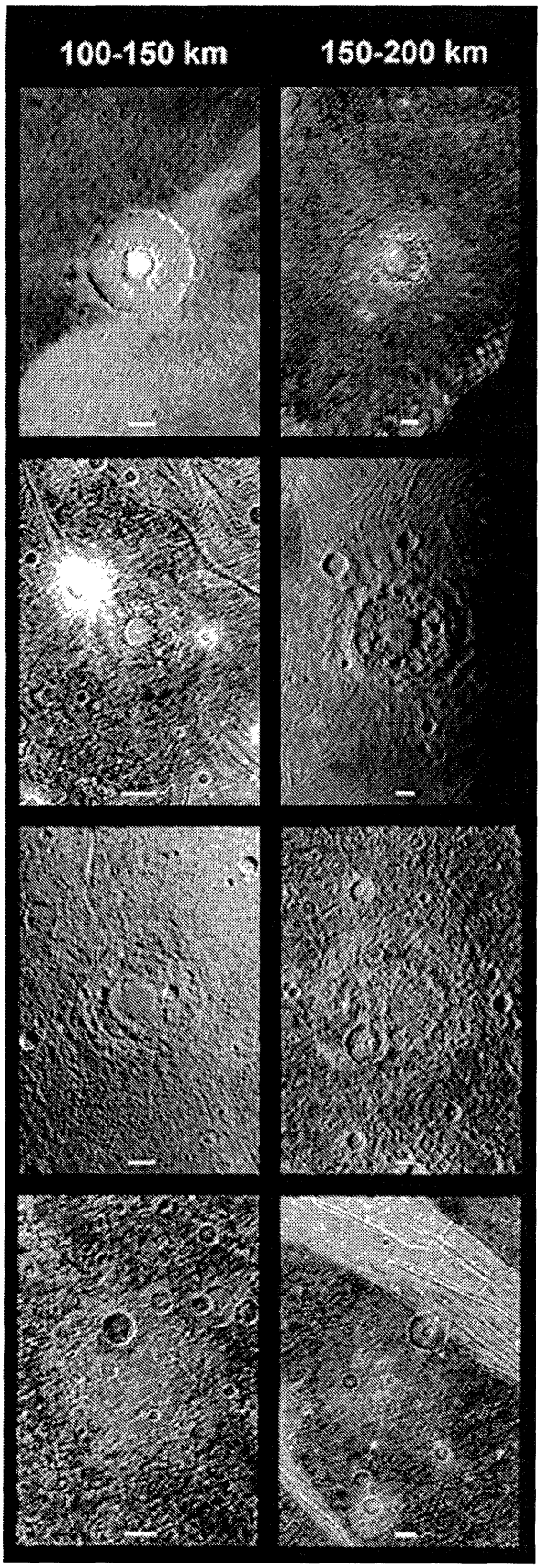

Figure 18.1. Impact crater morphologies on Ganymede at increasing age from top to bottom. Scale bars are 30 km. See Section 18.2.1 for descriptions and crater names.

et al. 1998, 2001). *Galileo* also extended the search for impact craters on Io with high-resolution imaging (Chapter 14). Finally, completion of global 3-km/pixel imaging of Ganymede and Callisto and high-resolution *Galileo* studies of selected type examples of large impact features on the Galilean satellites allow us to begin mapping global crater distributions and to test some of the models developed post-*Voyager*. One result is the completion of a global database for all craters on Ganymede, Callisto, and Europa down to crater sizes of 30, 50 and 1 km, respectively (compiled by P. Schenk). The data include crater morphology, size, shape (e.g., depth), location, relative ages (where determined), ejecta properties and dimensions, and the morphology and dimensions of structural features internal to the rim.

As on the rocky terrestrial planets, impact crater morphology on the icy Galilean satellites becomes increasingly complex with increasing crater size. However, larger craters on these satellites become progressively less like their rocky counterparts. Some larger impact features in particular (central dome craters, palimpsests, and Valhalla-class multi-ring features, for example), have no obvious analogs on other planets. Palimpsests in particular are so heavily modified or poorly preserved that it is difficult to identify structures (e.g., rim) or relate the structure and morphology of one class of impact crater to another. These larger impact features are also potentially more sensitive to differences or changes in internal properties at greater depths. Understanding of the origin of these features is relevant to modeling surface ages because the estimation of palimpsest diameters (and hence the size–frequency of larger impact features in general) is dependent on deducing the location of the equivalent crater rim.

The various studies of crater morphology on Ganymede and Callisto have resulted in a nonuniform crater nomenclature in the literature. In synthesizing crater observations, we put forward a revised and somewhat simplified crater nomenclature (treated in greater depth in Schenk and Moore, in preparation). We are aware that differences in scene illumination and image resolution can radically alter the appearance of textures and units.

18.2.1 Ganymede and Callisto

Figure 18.1 illustrates changes in morphology over time on Ganymede. Similar morphologies are observed on Callisto. Also shown are morphologies at two different diameters (increasing toward right). From top to bottom (left): Enkidu (central dome crater, $D = 123$ km), unnamed crater (anomalous dome crater, $D = 100$ km), Hathor (penepalimpsest, $D = 120$ km), and Edfu Facula (palimpsest, $D = 120$ km). From top to bottom (right): unnamed crater (central dome crater, $D = 178$ km), Serapis (anomalous dome crater, $D = 175$ km), Nidaba (penepalimpsest, $D = 180$ km), and Hermopolis Facula (palimpsest, $D = 166$ km). Palimpsest diameters are estimated rim diameters. Note the disrupted or missing southeastern rim section of the unnamed central dome crater at upper right, indicating partial collapse of malformation of the rim. All images have been scaled so that crater diameters appear similar in each image.

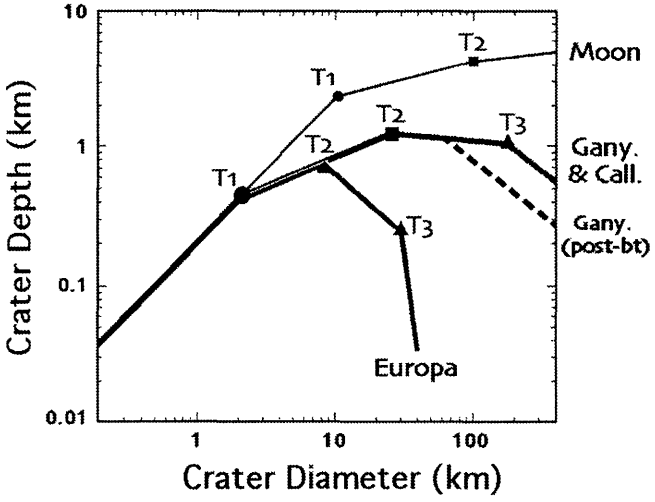

Figure 18.2. Schematic diagram of impact crater depth/diameter data for the Galilean satellites (heavy lines). Shown are least-squares fits to original data (presented in Schenk 2002). Lunar crater data (thin line) is shown for comparison (Pike 1977, Williams and Zuber 1998). T1, T2, and T3 identify changes in morphology and shape. T1 is the simple–complex transition, T2 is the change from complex to central pit and dome morphology. T3 is the transition to large basins or multi-ring morphologies. Dashed Ganymede line (post-bt) shows possible interpretation of depth/diameter curve for Ganymede during and shortly after the formation of bright terrain, based on differences in crater morphology and shape with time (see text). Significant features include the shallower depths for larger craters and the smaller transition diameters in comparison to lunar craters, and the unusual roll-over of large crater depths observed on the icy Galilean satellites. Also of note are the similarity of crater shapes on Ganymede and Callisto (Gany. & Call.) and the anomalously shallow crater shapes for craters larger than ~8 km on Europa.

Simple, Complex, and Central Pit Craters

Relatively fresh simple craters (<3 km diameter) on all three icy Galilean satellites are characterized by classic bowl shapes morphologically similar to simple craters on the Moon. Depth/diameter (d/D) ratios of simple craters on Ganymede and Callisto (Figure 18.2, Schenk 2002) average ~0.21 and ~0.19, respectively, similar to those on the Moon (Pike 1977). (The anomalously shallow d/D ratios for simple craters on Ganymede reported by Schenk (1991) were based on lower-resolution *Voyager* data in which the measured craters were less than ~10 pixels across. The "simple" crater depths were reasonably correct, or nearly so, but the craters were in fact complex craters not fully resolved by *Voyager*.)

Complex craters range from ~2 to ~35 km on Ganymede and Callisto and are morphologically similar to complex lunar craters, except for less extensive rimwall terraces (Schenk 1991). These craters are shallower than lunar complex craters by 40–70% (Schenk 1991, 2002), although the slope of the d/D curve in this diameter range is comparable to lunar complex craters. As on the Moon, this morphologic transition corresponds to a break in slope in the depth/diameter curves (referred to here as Transition I) on these satellites (Figure 18.2). For Callisto and Ganymede, Transition I diameters (based on the intersection of the depth/diameter curves in Schenk (2002)) are similar, 2.6 ± 0.5 and 1.9 ± 0.5 km (Figure 18.2), respectively, as compared to 9–11 km on the Moon (Pike 1988). (On Ganymede, the morphological transition diameter, or the diameter where central peak craters outnumber simple craters, is 2.1 ± 0.2 km (a total of 44 craters between 1 and 7 km in diameter were examined using the highest resolution (<100 m/pixel) images)).

Between ~35 and ~60 km in diameter, central pit craters are the normal crater morphology on Ganymede and Callisto, with a small rimmed central pit replacing the central peak (see Figure 18.1 for examples). Central pit craters are rarely if ever observed on the Moon or Mercury but superficially similar craters are occasionally observed on Mars. In contrast to complex craters, the depths of central pit craters are constant or decline slightly with increasing size. The change from central peak to central pit morphology correlates with the second break in slope, i.e., Transition II, in d/D curves for Ganymede and Callisto, which occurs at ~26 km on both satellites (Schenk 2002, Figure 18.2). Pits have been ascribed to vapor explosions, or drainage of impact melt (e.g., Greeley *et al.* 1982, Croft 1983). Whatever their origin, these rimmed pits must be considered as transitional to and genetically related to the more complex landforms observed in larger craters as described below.

Central Dome Craters

For craters larger than ~60 km, the impact crater story on Ganymede and Callisto deviates from the lunar counterpart (Figure 18.1). At least five different morphologic types have been identified in this size range (Passey and Shoemaker 1982, Schenk and Moore 1998, in preparation). Many of these craters are large enough to count small superposed craters on and establish relative ages (counts by P. Shenk), which appear to show that each type formed during distinct periods in satellite history.

The most recently formed craters between ~60 km and ~175 km across are central dome craters (Figures 18.1, 18.3), where central peaks and central pits are replaced by large circular central domes (e.g., Passey and Shoemaker 1982, Moore and Malin 1988, Schenk 1993), also referred to as small dome craters (Moore and Malin 1988). These domes have rounded profiles up to ~1.5 km high but at high resolution are characterized by web-like networks of narrow fractures (Figure 18.3). The domes themselves are surrounded by an annular ridge or, in larger craters, by a ring of rugged massifs, both of which are interpreted as structurally equivalent to pit rims in smaller craters. At least 105 have been identified on Ganymede and at least 47 on Callisto. We note that several very large and relatively young impact features on these satellites described below, including Gilgamesh and Lofn, may qualify as variations of this morphologic type.

Like central pits, the dome/crater size ratio increases with increasing crater diameter (Schenk 1993). Central dome crater depths range between 0.8 and 1.6 km. Together with central pit craters, these craters form a trend of constant or gently decreasing depths (Figure 18.2). The rims of most central dome craters larger than ~150 km and formed relatively recently (i.e., those devoid of superposed cratering in available images), such as Bran, on Callisto or the unnamed Ganymede crater in Figure 18.1 (upper right), are partially unformed or obliterated, however, suggesting that anoma-

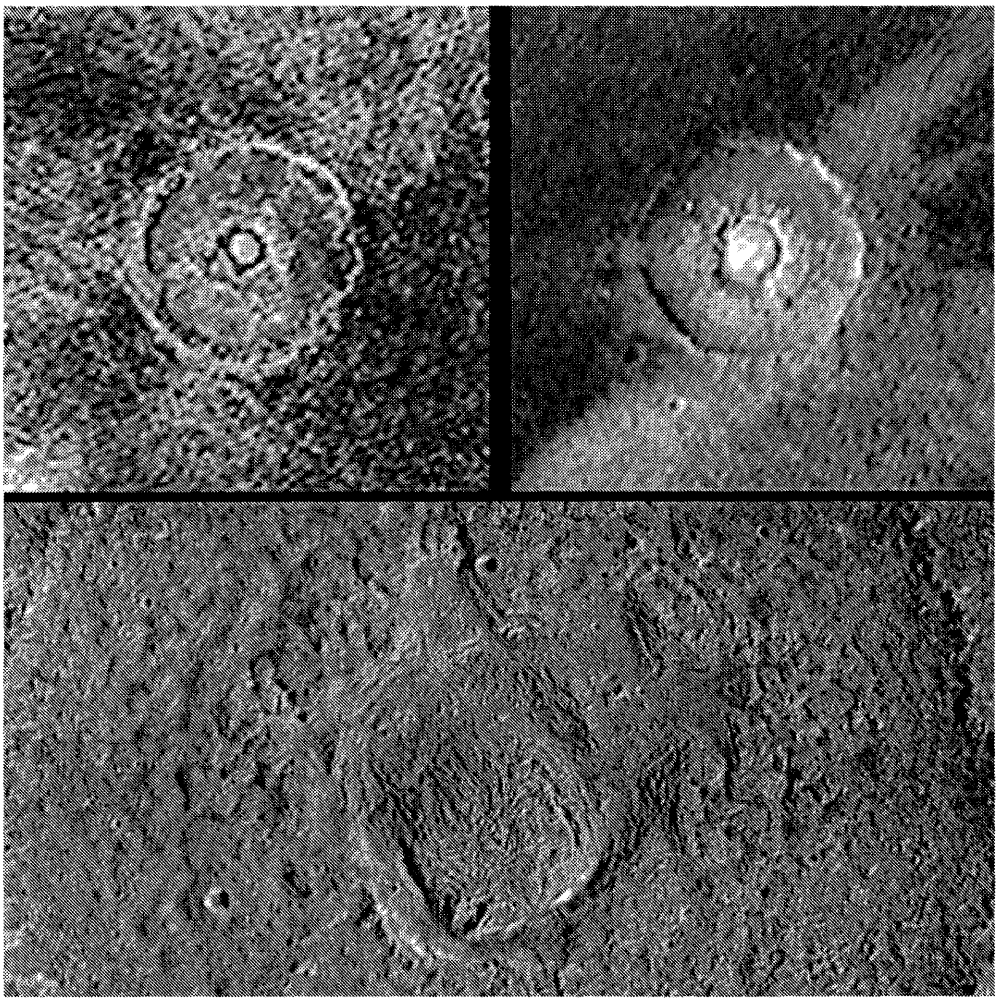

Figure 18.3. Central dome craters on Ganymede. Clockwise from upper left: Ninsum (D = 88 km), Enkidu (D = 123 km); and Melkart (D = 105 km). *Voyager* images of Ninsum and Enkidu show the general lack of rim terracing and the relatively bright rounded central dome. *Galileo* (~250 m/pixel) image of Melkart reveals a crenulated dome texture and a hummocky floor morphology reminiscent of much higher resolution Lunar Orbiter images of the lunar crater Tycho. Portions of Melkart crater rim are visible at upper left and upper right.

lous morphologies may be developing in the largest craters, as we discuss below.

Anomalous Dome Craters

Anomalous dome (AD) craters (also referred to as Type II penepalimpsests (Passey and Shoemaker 1982), or large dome craters (Moore and Malin 1988, Schenk 1993)) feature prominent, relatively bright, circular central domes surrounded by a ring of rugged massifs (Figures 18.1, 18.4), and are "anomalous" on that they generally lack morphologically coherent rim scarps. A total of 42 anomalous dome craters have been identified on Ganymede between 50 and 175 km in diameter, and 60 on Callisto between 50 and 250 km diameter.

Anomalous dome craters resemble central dome craters, except in three respects. First, as described above, they lack coherent rim structures. Rather, rim morphology is characterized by a very broad, low rise (e.g., Neith on Ganymede), incomplete outward- or inward-facing scarp segments (e.g., Doh on Callisto), or no rim expression at all (e.g., Anzu on Ganymede) (see Figures 18.4 and 18.10, bottom left). Rim location is consistent with scaling of continuous ejecta deposit dimensions, which are usually easily mapped from secondary crater distributions (Schenk and Ridolfi 2002, and discussed later). Second, the ratio between dome and rim diameter for these craters (whether observed or estimated from ejecta deposit scaling) is roughly constant at ~0.4, regardless of crater size. Third, most anomalous dome craters are generally not associated with bright ray or floor deposits and have somewhat higher superposed crater densities compared to central dome craters. While this suggests that anomalous dome craters are generally older than central dome craters, ejecta deposits and secondary craters of those AD craters near or on bright terrain on Ganymede are clearly superposed on to bright terrain (no similar benchmark horizon exists for Callisto). Thus, anomalous dome craters formed after bright terrain materials were emplaced on Ganymede (which may have occurred over an extended interval of geologic time), but are probably not forming today.

Rim-to-floor depths of anomalous dome craters are very

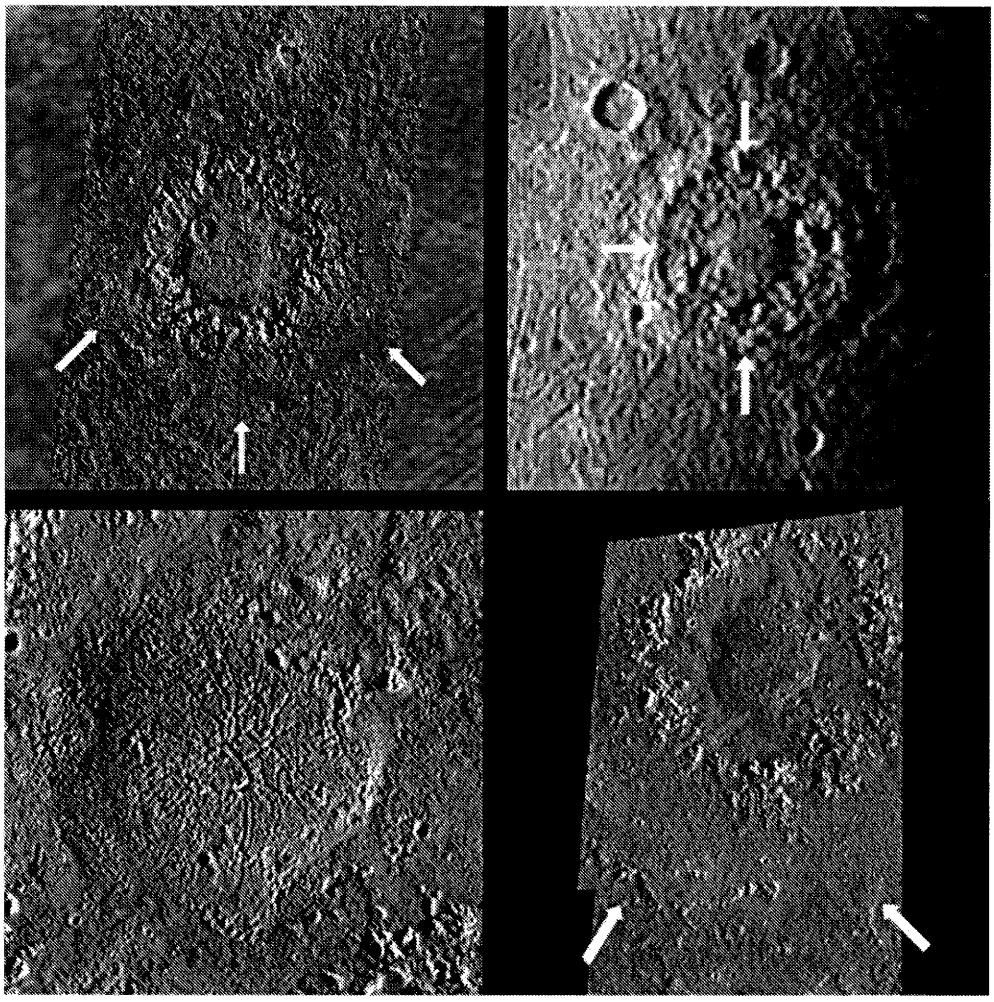

Figure 18.4. Anomalous dome craters on Ganymede and Callisto. Clockwise from upper left: Neith, Ganymede ($D = 165$ km); Serapis, Ganymede ($D = 175$ km); Doh, Callisto ($D = 115$ km); and close-up of 25-km-wide central dome of Doh. Arrows identify remnant crater rim or predicted rim locations. These craters are characterized by large rounded domes surrounded by annular zones of massifs. They resemble central dome craters (Figure 18.3), except for the anomalous rim morphology and tendency toward somewhat higher superposed crater densities.

difficult to determine, but are generally much shallower than for central dome craters. Often, the rim cannot be identified, suggesting a negligible crater depth. In cases where portions of the rim can be identified, the relief is only a few hundred meters. This apparent decrease in effective crater depths has been interpreted as evidence for an additional transition (Transition III) in the depth/diameter curves of Ganymede and Callisto (Figure 18.2, Schenk 2002). The prevalence of anomalous dome crater morphology down to diameters of only ~60 km suggests that Transition III may have occurred at ~60 km in the time of anomalous dome crater formation. Incipient anomalous dome morphology on Ganymede and Callisto occurs in younger central dome craters only at diameters of ~150 km or larger (Figure 18.1), suggesting that Transition III has changed and is larger (≥150 km) at the present time (Figure 18.2).

Penepalimpsests

Penepalimpsests (Passey and Shoemaker 1982) resemble classic complex craters even less than do anomalous dome craters (Figures 18.1, 18.5). Penepalimpsests are defined by circular high-albedo patches on Callisto and on dark terrain of Ganymede, but have similar albedoes to bright terrain when formed on it. Where observed under low-sun illumination, the margin of this albedo unit is often defined by an outward-facing scarp less than a few hundred meters high. A total of 11 have been identified on Ganymede between 60 and 210 km in diameter, and 3 on Callisto between 180 and 350 km diameter. These include the *Galileo* Ganymede high-resolution imaging targets Epigeus, Zakar, and Buto Facula.

Mapping of secondary craters shows that the limit of continuous ejecta is separated some distance from the outer bright margin (Figure 18.5). Several concentric structures, usually inward-facing scarps or narrow low ridges several hundred meters high, as well as a central smooth area, can be identified in penepalimpsest interiors. Scaling from the ejecta blanket dimensions (Schenk and Ridolfi 2002, Section 18.3.4) allows us to understand these features and map out the nominal rim location. The diameter of the outermost of the concentric interior structures corresponds with the

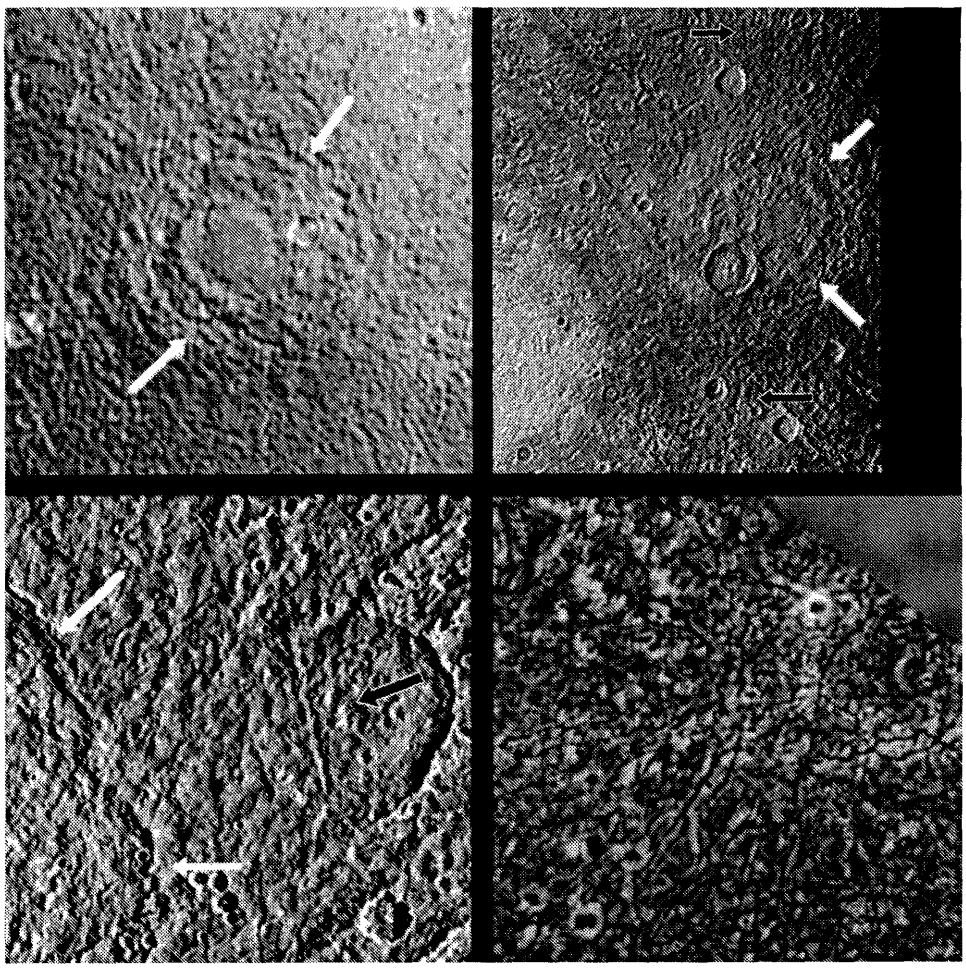

Figure 18.5. Penepalimpsests on Ganymede. Clockwise from upper left: Hathor (D = 120 km); Nidaba (D = 180 km); close-up of fissures and lineations in central region of Epigeus (D = 210 km) (image width ~27 km); and close-up of eastern rim and ejecta deposit of Buto (D = 157 km). White arrows mark crater rim in each case. Black arrows at Nidaba show edge of continuous ejecta deposit as defined by extent of secondary craters. Black arrow at Buto marks edge of inner ejecta facies, where 40-km-wide older crater is partially buried.

expected location of the crater rim (Schenk and Moore, in preparation). Hence, the outer margin of the bright circular albedo patch in this interpretation corresponds to the inner or pedestal ejecta facies. Although relatively flat, the central smooth areas are proportionally similar in size and therefore regarded as the equivalent to central domes in younger craters. Intricate fracture networks similar to those on central domes are visible on the surfaces of these central smooth spots in high resolution images of both *Galileo* targets Epigeus and Buto Facula (Figure 18.5), consistent with this interpretation.

When penepalimpsests are near or on Ganymede's bright terrain, ejecta deposits and secondaries overlap and thus postdate bright terrain. Superposed crater densities are very similar to those on bright terrain (Figure 18.6), however, suggesting that these structures are either coincident with or just postdate bright terrain (Schenk and Moore, in preparation). In fact, one penepalimpsest near the south pole, Teshtub, is partially truncated by a relatively young lane of smooth bright terrain (DeHon *et al.* 1994).

Squyres (1980) based on a simple photoclinometric model suggested that Zakar was domically uplifted by ~2 km. New stereo measurements by one of us (P. Schenk) of another penepalimpsest, Hathor (Figure 18.5), and an anomalous dome crater (at 39° S, 146° W) confirm that the surfaces of these impact features are raised 1–2 km in elevation above surrounding plains, consistent with impressions from low-sun images (Figure 18.4, upper right). Despite this, less than ~500 m of rim relief is observed within penepalimpsests, less than half that typical of central dome craters.

Palimpsests

The most enigmatic impact features on Ganymede are the circular high-albedo features termed palimpsests (Figures 18.1, 18.7) (Passey and Shoemaker 1982). A total of 37 have been identified on Ganymede (with all residing on dark terrain, which covers 34% of Ganymede), and 8 on Callisto. (It should be noted that palimpsests are more difficult to distinguish from penepalimpsests on Callisto due to the lower resolution of the imaging coverage.) An outward-facing topographic scarp or step is often visible along the edge of the high albedo unit but relief in the interior is extremely subtle. Crater rims are not recognizable, but

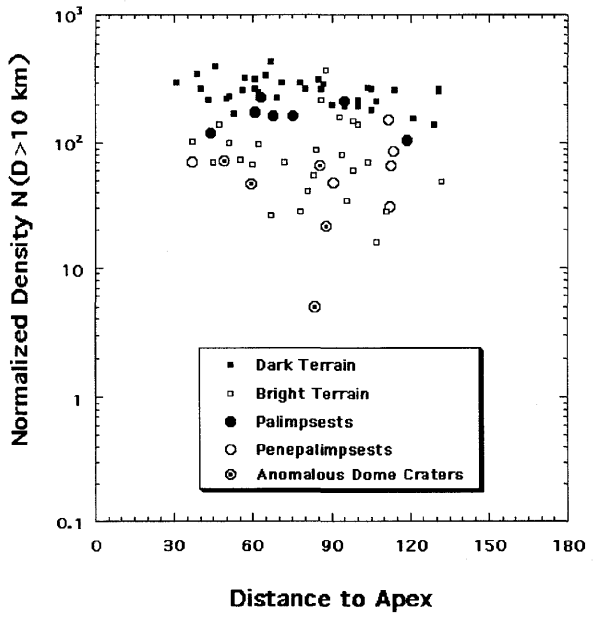

Figure 18.6. Normalized crater densities per 10^6 km^2 for dark and bright terrains and various impact crater types on Ganymede. These are plotted as a function of distance to apex of orbital motion in order to account for the global asymmetry in crater density (Zahnle *et al.* 2001). Palimpsests tend to be intermediate in crater density and inferred age between dark and bright terrain. Penepalimpsests are similar in density to bright terrain, while anomalous dome craters can be similar to or lower in density than bright terrain (several anomalous craters plotted below the margins of this chart). Central dome craters have effectively zero superposed crater densities ($D > 10$ km), and are not plotted.

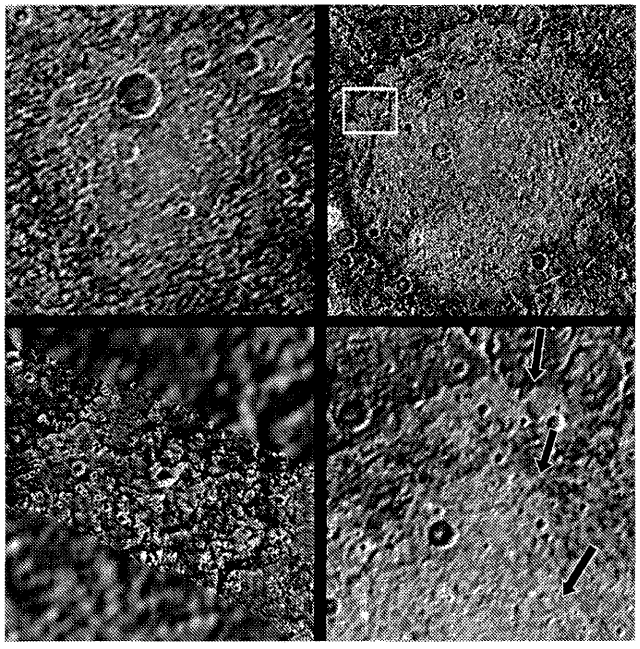

Figure 18.7. Palimpsests on Ganymede. Clockwise from upper left: Edfu Facula (outer margin $D = 185$ km; rim $D = 118$ km); Memphis Facula (outer margin $D = 355$ km; rim $D = 245$ km); close-up of northern section of Memphis Facula showing concentric zoning; *Galileo* high-resolution close-up of outer edge of Memphis Facula (scene width ~50 km; location shown as white box in upper right view). In the bottom right view, the outer zone of Memphis Facula (between upper arrows) is relatively darker than the central region. Bottom arrow indicates a more rugged annulus marking the boundary of the central smooth area, which we interpreted to be equivalent to a central dome complex.

faint concentric lineations and central smooth areas can sometimes be recognized in larger palimpsests. Secondary craters are generally not mappable against the heavy background cratering characteristic of dark terrain, but this is not surprising given the degree of mass-wasting now evident from *Galileo* on older terrains on both satellites (Prockter *et al.* 1998a, Moore *et al.* 1999). Palimpsests thus resemble highly flattened penepalimpsests (Figure 18.5, 18.7), except palimpsests are truncated by and have higher crater densities than bright terrain but slightly lower than dark terrain (Figure 18.6). Palimpsests thus predate bright terrain.

Palimpsests and penepalimpsests have often been lumped together (e.g., Thomas and Squyres 1990, Jones *et al.* 2003), but palimpsests occur only on older terrains, have less morphologically distinct concentric zonal organization, no mappable or preserved ejecta deposits, and are very subdued topographically. Penepalimpsests occur on all terrain types, have topographically expressed concentric features, and mappable ejecta or secondaries. The difference therefore appears to be related primarily to age, with bright terrain formation separating the two types (Figure 18.6).

Lofn

Lofn is one of the most distinctive craters on Callisto (see Figure 17.28 in Chapter 17). Identified as a large bright patch in *Voyager* images (Schenk 1995), *Galileo* revealed a large circular massif ring surrounding a smooth central area (Greeley *et al.* 2001). No discrete rim can be identified, but secondary craters can be clearly mapped roughly 365 km from the center. Between the secondaries and the central features lies a sparsely cratered smoothed zone resembling the ejecta deposit of Gilgamesh (see next section). Extending outward from this zone is a set of diffuse bright rays. The superposition of smaller craters indicates that Lofn may be at least 2 Gyr old (Wagner *et al.* 1999 and Section 18.5.6), suggesting that these rays may be at least partially compositional in nature rather than exposures of fresh ice or frost. Greeley *et al.* (2001) estimated the rim diameter to be ~180 km and ascribed the morphology to impact of a fragmented projectile or impact into ductile substrate. The true rim-equivalent diameter, as derived from ejecta scaling (Schenk and Ridolfi 2002), is more likely ~355 km, strengthening the case for impact into a ductile substrate, as discussed below. Morphologically, Lofn is considered equivalent to an unusually large central dome or an anomalous dome crater, and is the largest non-multi-ring crater on either Ganymede or Callisto. The lack of a coherent rim is consistent with either analog.

Multi-ring Structures – Orientale Class (Gilgamesh)

At least one large impact feature on Ganymede and Callisto shares some commonality with multi-ring basins on the Moon, exemplified by the Orientale basin. At 590 km diame-

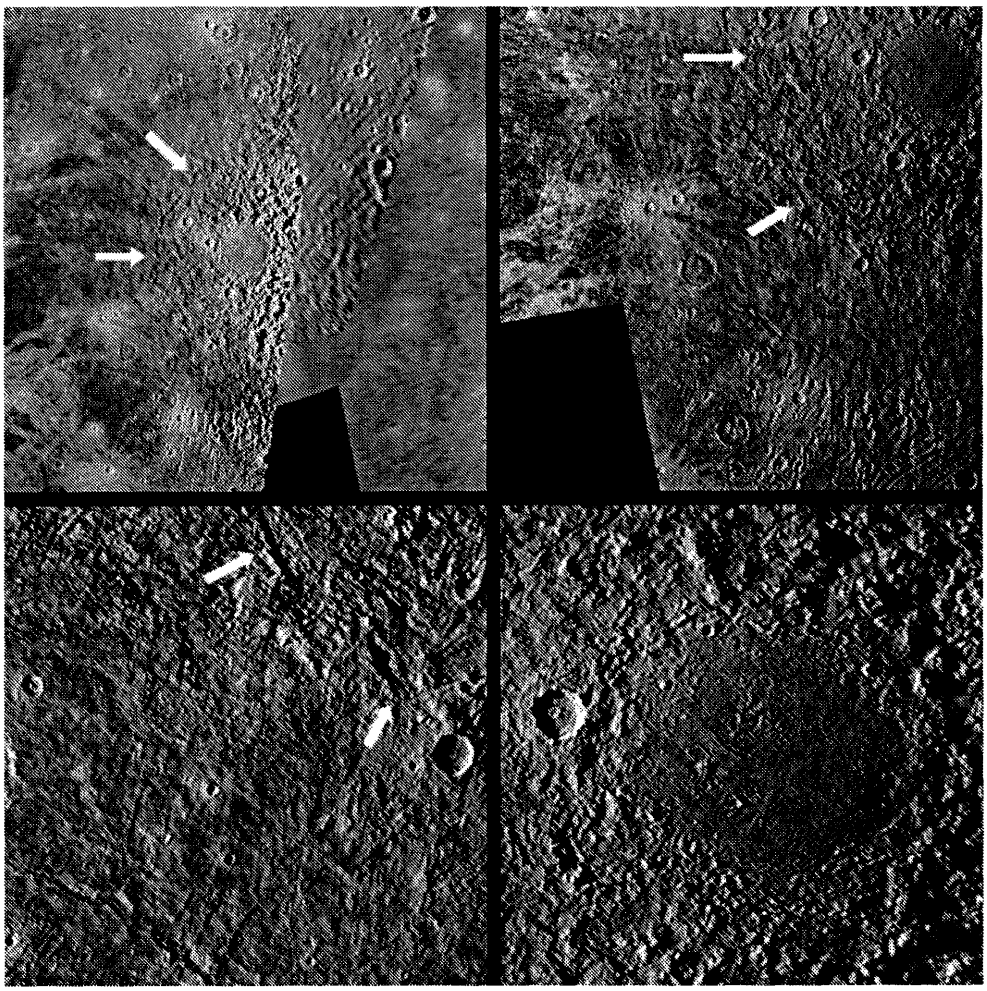

Figure 18.8. Gilgamesh multi-ring impact structure, Ganymede. Upper left: Synoptic orthographic mosaic of *Voyager* (left) and *Galileo* (right) images centered on Gilgamesh (D = 585 km). Horizontal dimension ~1500 km. Upper right: Detail of southwest quadrant of structure illustrating the central smooth region, inner massif zone, rim (arrows), and ejecta deposit. Secondary crater chains are apparent beyond the edge of the ejecta deposit at bottom. Note that secondary craters are absent in the western sector, indicative of oblique impact. Lower right: Detail view of central smooth region showing subradial lineations superficially similar to features seen in central domes. Lower left: Detail of rim region and ejecta deposit. Arrows indicate location of Gilgamesh rim.

ter, Gilgamesh is by far the largest impact feature fully preserved on Ganymede (Figure 18.8); the next largest recognizable impact feature on Ganymede is only ~350 km across. *Voyager* imaged the western two-thirds of Gilgamesh at low Sun and sub-kilometer pixel resolution, providing excellent topographic discrimination. *Galileo* obtained low resolution coverage over the eastern portion of the ejecta deposit, and high sun, low phase images of the basin interior.

Gilgamesh consists of at least 3 concentric zones and 4 concentric structural rings (Figure 18.8). The smooth central zone ~150 km across has a domical surface rising asymmetrically up to ~500 m (Figure 18.8). This area is surrounded by a discontinuous inward-facing quasi-concentric scarp ~1 km high on average (elevations are from stereo mapping, Schenk *et al.* 1997). This scarp marks the inner margin of a 225-km-wide annular zone of hummocky terrain punctuated by rugged, somewhat angular massifs and quasi-concentric but discontinuous ridges. The outer limit of this zone coincides roughly with a prominent contiguous concentric inward-facing scarp ~1 km high on average (locally up to 1.5 km high) and ~585 km in diameter (Figure 18.8). Although concentric, the outline of this scarp has some quasilinear segments, suggesting some control by pre-existing structural trends. The location and prominence of the 590-km scarp indicates it is probably the crater (or basin) rim.

Extending beyond the apparent rim is an annular zone ~200 km wide of mottled texture in which pre-existing grooved terrains have been obliterated or mantled (Figure 18.8). This is clearly the continuous ejecta deposit, beyond which lie numerous large oblong secondary craters and crater chains. No secondary craters are recognizable in the western quarter of Gilgamesh, suggesting that Gilgamesh formed by an oblique impact, with an impact angle possibly between 10 and 30° (e.g., Gault and Wedekind 1978). Within this unit lies a second but less prominent concentric inward-facing scarp 0.5 to 1 km high and ~750 km in diameter. Near the edge of this unit is a sinuous trough or furrow more or less concentric to Gilgamesh. This single furrow, at a diameter of ~980 km, is probably a fracture or graben and

resembles some of the outer furrows of the Valhalla structure on Callisto.

The inner scarp, 590-km scarp, 750-km scarp, and outer furrow form a set of four widely spaced but discrete ring structures, giving Gilgamesh a resemblance to multi-ring features such as Orientale (Passey and Shoemaker 1982). It remains the only such feature identified on the Galilean satellites. There are major differences, however, including the unusually chaotic zone between the rim and the inner ring. Also, Gilgamesh is not more than 2 km deep, in contrast to Orientale which is 6–8 km deep (Williams and Zuber 1998).

Despite its great size and complex structure, Gilgamesh appears to possess many of the basic features found in smaller craters on Ganymede. Aside from the well preserved ejecta blanket, the inner massif zone and central smooth area are similar in relative diameter to the crater rim, as are the massif rings and central dome complexes observed in central dome and anomalous dome craters. Indeed, the network of bright lineations crossing the central smooth deposit in *Voyager* images of Gilgamesh is reminiscent of the networks of lineations in ordinary central domes (Figure 18.4), consistent with a central dome analogy for the center of Gilgamesh.

Multi-ring Structures – Valhalla Class

Most impact features larger than 350 km on Ganymede and Callisto are of the Valhalla-class multi-ring type (McKinnon and Melosh 1980, Passey and Shoemaker 1982, Schenk and McKinnon 1987, Prockter *et al.* 1998b). These differ from Gilgamesh and consist of numerous (>5) concentric ring structures which are usually 10–30 km apart and are more closely spaced than Gilgamesh or Orientale type rings (Figure 18.9). Smaller structures consist of concentric graben-like rings. Fully developed features such as Valhalla have two morphologies: the outer graben and an inner set of V-shaped ridges and valleys (the morphology of these features is described more fully in Chapter 17). Relief across ridges and scarps can be 2–3 km (Schenk 1995). On Ganymede and Callisto these features are relatively old (Passey and Shoemaker 1982); all such features on Ganymede occur on older dark terrain.

Due to *Galileo* data restrictions, these multi-ring features did not receive their due attention, and our global mapping must be regarded as incomplete. The degraded nature of these older features and the fragmental preservation of these features on Ganymede's dark terrain makes identification and reconstruction of these systems doubly difficult. Analysis of returned data is also incomplete.

Particularly vexing has been the issue of estimation of original or nominal rim diameters. The morphologic similarity of most of the ring arcs makes identification of the original rim impossible by direct examination. The best tool for diameter estimation is ejecta and secondary crater mapping (Schenk 1995). Secondaries, as in the case of Valhalla, can be identified by size, clustering, and by elliptical or tear-drop shapes. Ejecta can be mapped by the relative reduction in the number of small craters, or as an albedo feature concentric with the ring system. Even these can be difficult to map in the most degraded structures. To date, 6 Valhalla-class features are known on Callisto (at least 2 of which are >300 km across), and 5 on Ganymede (at least 4 of which are >300 km across). The largest are Valhalla ($D \sim 1000$ km) on Callisto, and the Galileo-Marius Regio ring system on Ganymede (diameter uncertain but probably larger than 2000 km). Only two are known on Europa. These two examples, Tyre (Figure 18.9) and Callanish (Chapter 15), at ~33 and ~41 km respectively, are similar morphologically, but much smaller than their Ganymede and Callisto counterparts. Because they are much better preserved than those on the other satellites, they should serve to improve our understanding of ring formation. Ring systems whose diameters can be mapped with some confidence have been included in our global crater counts described in later sections.

Despite their partially preserved record, it is clear that multi-ringed structures represent a distinctly different phase in the evolution of Ganymede and Callisto. The basic inference from McKinnon and Melosh (1980) that these represent impact into a relatively thin lithosphere remains robust. In this scenario, the lithosphere at the time of these larger impacts is fractured as the underlying material flows inward to viscously fill the original impact cavity (see Melosh 1989, Chapter 9). If the lithosphere is very thin with respect to the crater, the cavity will fill completely and the shell will fracture much more extensively than in a relatively thick lithosphere. The lack of such features in post-bright terrain craters and young large craters on Callisto suggests that lithospheres subsequently thickened on these bodies. Despite this, the picture remains incomplete. Numerical modeling is required in order to estimate how thin the lithosphere must be in order to develop Valhalla-class rings. The global survey at 100 m or better resolution must be completed in order to map out when these features formed and how large they were.

18.2.2 Europa

On Europa, the impact crater size–morphology spectrum is both truncated and compressed in diameter space relative to Ganymede and Callisto (Figures 18.2, 18.10). Although similar at smaller sizes (top of Figure 18.10), crater morphology on Europa becomes progressively more divergent from Ganymede at larger diameters (bottom of Figure 18.10). (Shown in Figure 18.10 are the following europan craters (from top to bottom): Brigid ($D = 9$ km), Grainne ($D = 14$ km), Pwyll ($D = 27$ km), and Tyre ($D = 41$ km). Ganymede craters (from top to bottom): unnamed crater ($D = 15$ km), unnamed crater ($D = 30$ km), Enkidu ($D = 123$ km), and Anzu ($D = 155$ km). All images have been scaled so that crater diameters appear similar in each image. A total of 150 craters on Europa larger than 1 km across were cataloged by P. Schenk) The morphology of smaller craters is similar on all three satellites but the largest observed crater on Europa is only ~40 km, so impact features such as central domes and penepalimpsests might not be expected. Also, only 15% or so of the surface has been imaged at better than 1 km/pixel, the minimum required to classify most impact craters on the satellites.

Depth/diameter ratios of simple craters on Europa average ~0.17, slightly lower than on Ganymede or Callisto, although numerous craters have depth/diameters of ~0.2 (Schenk 2002). A total of 16 complex craters are known on Europa, ranging from ~3 to 27 km in diameter (Moore *et al.* 1999). Moore *et al.* (2001) report that the transition from simple to complex morphology (Transition I) on Europa

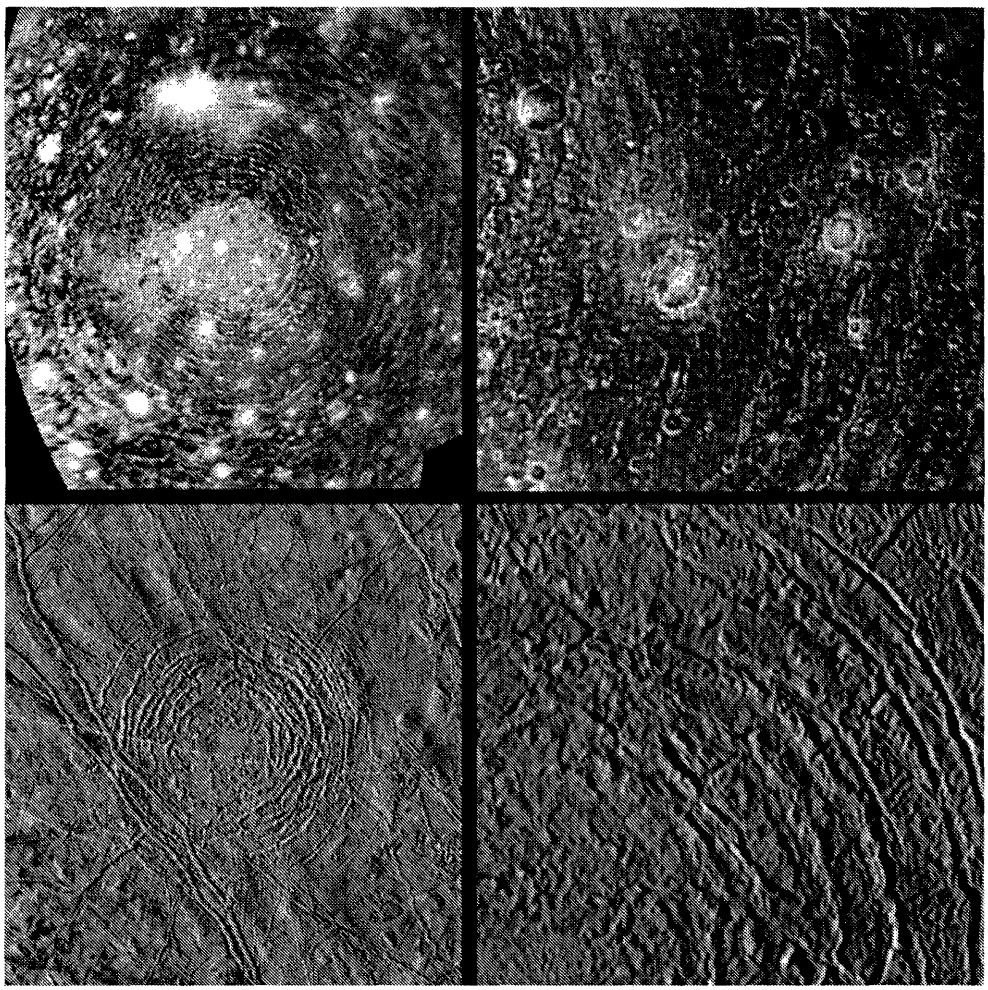

Figure 18.9. Multi-ring impact features on Callisto and Europa. Upper left: *Voyager* orthographic mosaic of Valhalla, Callisto (D = 1000 km; ring system diameter ~3000 km). The central bright zone is a crater floor deposit superposed on individual ring structures. The effective rim location lies just beyond this bright deposit. Scene width ~2700 km. Upper right: *Voyager* mosaic of eastern portion of Valhalla showing inner ridge zone (left) and outer graben zone (right). Scene width ~750 km. Lower left: *Galileo* orthographic mosaic of Tyre, Europa (D = 41 km; ring system diameter ~170 km). Scene width ~240 km. Lower right: close-up of northeast quadrant of Tyre, showing transition from central smooth region to ridges to graben-like fractures. The effective rim diameter lies within the innermost prominent concentric ridges at bottom center. Secondary craters at upper right mark the outer limit of the continuous ejecta deposit. Scene width ~65 km.

(based on the presence or absence of central peaks) occurs at ~5 km, higher than reported here for Ganymede and Callisto. This value may be misleading as most of the craters identified in the 3–5 km size range were deeply shadowed and small central peaks may have been obscured. From Schenk's (2002) data, the d/D intercept on Europa for simple and complex craters occurs at ~3.9 km, but this is also misleading as complex crater depths overall decrease with increasing diameter. Between 3 and 9 km diameter, however, the depths of complex craters on Europa increase and are comparable to similar-sized complex craters on Ganymede and Callisto. The d/D transition diameter for simple craters and complex craters <9 km across on Europa is ~3.3 km (Schenk 2002), more similar to Ganymede and Callisto.

At diameters >9 km, crater morphology on Europa begins to diverge from that on its Galilean siblings (Moore *et al.* 1998, Schenk 2002). Beyond this, complex crater depths on Europa are shallower than their counterparts on Ganymede, and as noted above decrease with increasing diameter (Figure 18.2). In addition, central peaks become progressively more complex or degraded with increasing diameter, resembling modified or partially developed central pits, especially in the four largest complex craters (Amergin, Gráinne, Pwyll and Manannán, see Figure 18.10). Similarly, crater rim morphology in these craters becomes progressively less well expressed (Moore *et al.* 1999), with discontinuous rims of variable height. The break in d/D slope and beginnings of morphologic changes at ~9 km constitutes the europan equivalent of Transition II.

Transition III on Europa occurs at $D \sim 30$ km (Figure 18.2) and correlates with the relatively abrupt development of multi-ring morphologies in the two largest known impact features, Callanish and Tyre (Figure 18.9). Like other Valhalla-class features, these structures are characterized by multiple concentric inner ridges and outer graben (Moore *et al.* 2001), but no central structures such as pits or domes

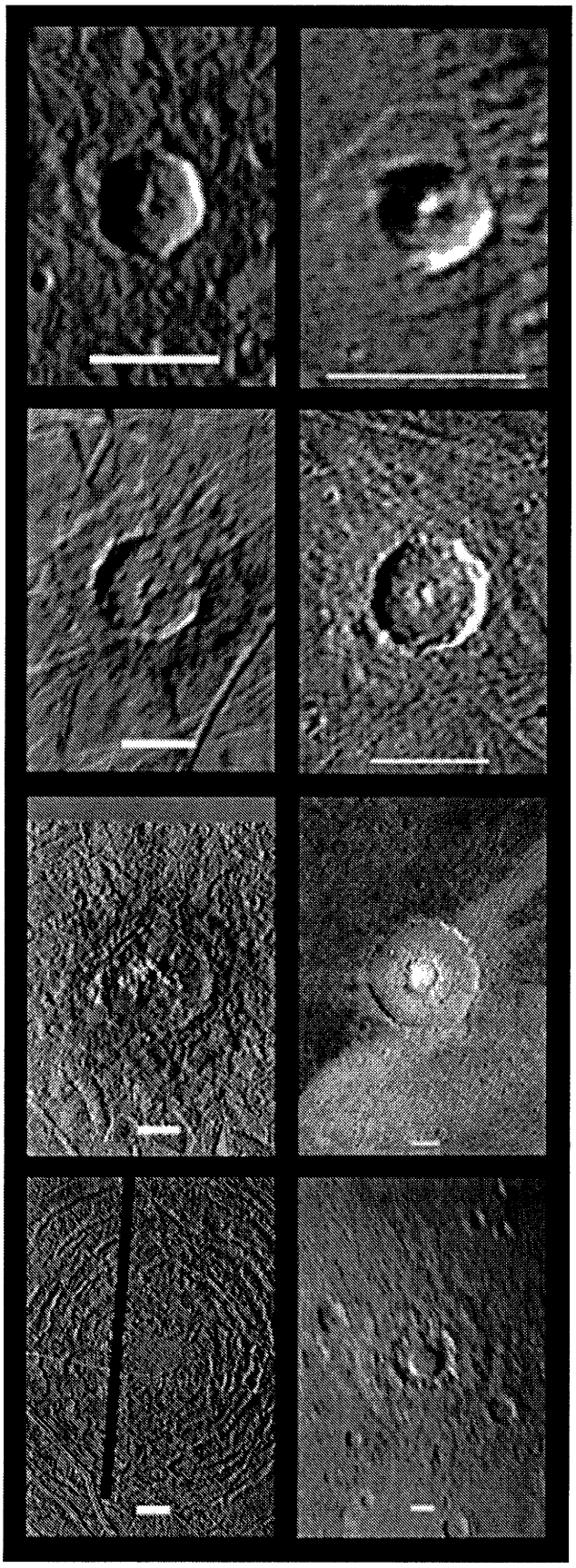

Figure 18.10. Impact crater morphologies on Europa (left, scale bars are 10 km) and Ganymede (right, scale bars are 30 km). See Section 18.2.2 for descriptions and crater names.

can be identified (Figure 18.9). Both Callanish and Tyre are recognized in low resolution images as circular dark spots that at higher resolutions correspond to the outer limit of the inner, or pedestal, ejecta facies. The sizes of Callanish and Tyre are difficult to determine due to the lack of demonstrable rim segments. Schenk (2002) estimated their rim-equivalent diameters by scaling from mappable ejecta deposits and secondary craters. Maximum relief across both structures does not exceed ~100 meters (from 2-D photoclinometry by Moore *et al.* 2001 and Schenk 2002). Most of these ridges and graben-like rings lie outside the nominal rim location and should not be attributed directly to rim slumping or floor uplift.

Of the 150 cataloged craters on Europa, 33 could not be classified due to resolution or illumination conditions, and 5 of these could be larger than 20 km across. Examples include Morvran, Taliesin, and Tegid, some of which may or may not have central domes (see Moore *et al.* 2001), a class of crater not otherwise observed on Europa. Some of these larger craters could be transitional between complex craters and multi-ring basins (Moore *et al.* 2001) and may thus prove important in detecting and defining changes in crater morphology and transitions over time. It falls to a future Europa mapping misssion to search out and map these craters and elucidate their story.

18.3 TOWARD A UNIFIED PICTURE OF IMPACT CRATERING ON THE GALILEAN SATELLITES

Morphologic changes can now be directly correlated with topographic changes in crater shape for Ganymede, Callisto and Europa (Schenk 1993, 2002), and the observations outlined above point to major morphologic changes on at least one satellite over time (Passey and Shoemaker 1982, Schenk 2002, Schenk and Moore 1998, in preparation). The resulting synergy leads us to a new paradigm in which a complex size–morphology–age spectrum of crater types on all 3 satellites is linked to thermal stratigraphy and thermal evolution of their interiors. Before exploring this in detail, we first examine the origins of several controversial aspects of impact features on these satellites.

18.3.1 Viscous Relaxation

At least one pre-*Voyager* prognostication envisioned smooth icy worlds devoid of topography due to the rapid viscous creep of ice (i.e., Johnson and McGetchin 1973). Despite initial analyses of craters on Ganymede and Callisto favoring extensive viscous relaxation (e.g., Passey and Shoemaker, 1982), improved crater shape measurements (Schenk 1991, 2002) have shown that this mechansim is not as predominant as proposed. Much of the relatively shallow crater topography (relative to the Moon) observed on Ganymede and Callisto is now thought to be due to enhanced rim and floor collapse in low-strength icy lithospheres during crater formation (e.g., Schenk 1991). Highly flattened craters with profiles characteristic of relaxation do occur in older dark terrains on Ganymede and Callisto and in some areas may account for over half the observed crater population (Figure 18.11). But relaxed craters are not ubiquitous and are rare on resurfaced terrains such as bright terrain or young impact

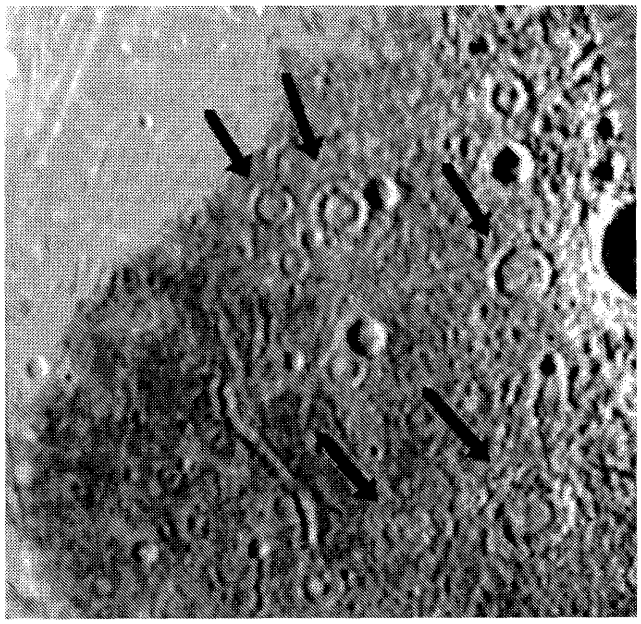

Figure 18.11. *Galileo* view of relaxed impact craters (arrows) on Perrine Regio, Ganymede. Fresh craters (highlighted by deep rim shadows) appear deep, but the oldest craters are topographically subdued. Craters in bright terrain (upper left) are pristine and have not been relaxed. View is ~800 km across.

features. Younger craters follow well-defined depth/diameter trends on these satellites, and show no evidence of relaxation after the time of bright terrain formation. Further, Woronow *et al.* (1982) argued that large crater erasure by relaxation does not explain the observed spatial distribution on Callisto (see discussion in Chapman and Mckinnon 1986). Also, long-term viscous flow may not be the most likely explanation for the anomalous morphologies of larger europan craters (Schenk 2002). The fundamental reasoning is that the non-lunar-like rim and central structure morphologies of Ganymede and Callisto cannot be produced from simple flattening of original lunar-like complex crater landforms. They are more likely to be primary morphologies formed during the impact event. Thus extensive viscous relaxation appears to be mainly limited to the early histories of these satellites.

Our understanding of the physical process of viscous relaxation has also changed in the last 20 years. Finite element modeling by Thomas and Schubert (1988) seemingly confirmed the earlier predictions of wholesale loss of all topography within millions of years, despite obvious evidence for preserved relief of several kilometers. Hillgren and Melosh (1989) argued that the elastic strength of ice preserves topography against viscous flow. These earlier studies suffered from the use of lunar crater shapes as their initial topography, imposing much higher driving stresses than are required by more recently determined crater shapes (Schenk 1991, 2002), and the use of ice-flow laws that did not completely describe the creep mechanisms responsible for ice deformation. Dombard and McKinnon (2000) revisited the issue and found that grain-size-sensitive creep (Durham and Stern 2001) dominates ice flow under current Ganymede conditions and that craters can be retained over the age of the solar system for low enough heat flows. The remaining step is to determine what heat flow conditions may be responsible for the relaxed craters we do see in older terrains.

18.3.2 Origin of Catenae

Large crater chains, or catenae, several hundred km long on Callisto resemble secondary crater chains but suitable source impact basins are lacking, with one or two exceptions (Passey and Shoemaker 1982, Schenk *et al.* 1996). In 1993, it was independently realized by H. J. Melosh and P. Schenk after the discovery of D/Shoemaker–Levy 9 that comets disrupted by passage close to Jupiter would form linear crater chains if they were to strike one of the jovian satellites immediately after tidal disruption (Melosh and Schenk 1993). In any later encounters with satellites the individual fragments will have drifted too far apart for a catena to form. Hence, on a synchronously rotating satellite, all primary impact catenae formed by disrupted comets occur on the hemisphere that faces towards the planet (more correctly, the actual catenal pole is rotated some number of degrees toward the apex of motion (McKinnon and Schenk 1995)). The distribution of the 8 known catenae on Callisto is consistent with this picture (Schenk *et al.* 1996). No unusual catena have been identified on Europa, but this is not surprising given the very low overall crater density (see below). The case of Ganymede is more complex as several of the 11 or so candidate catenae occur on the backside (see Section 18.4.4). There is some uncertainty regarding the origins of these smaller "uncooperative" catenae, however, which are less than 100 km long and could be secondary craters from one of the distant large impact craters. One large bright rayed catena at longitude 277° W is most likely a relic of a disrupted comet and implies nonsynchronous rotation at some time in the recent past. Further analysis is required to understand the origins of all of Ganymede's catenae, however.

18.3.3 Origin of Central Domes

Central domes (Figures 18.3, 18.4) are unique to Ganymede and Callisto and were a priority target for *Galileo*. *Voyager* observations led to several models for their origin, ranging from refrozen impact melt (Croft 1983), to post-impact diapirism (Moore and Malin 1988), or to rapid uplift of deep material during impact as is mapped in terrestrial impact craters (Schenk 1993). *Galileo*'s high-resolution observations revealed dense networks of narrow intersecting fractures on dome surfaces, but also failed to show relationships indicative of flooding or embayment by melt, thus favoring diapirism or rapid uplift. Rapid uplift of ductile material from depth during impact (Schenk 1993) is favored by two observations: the covering of crater floors and central domes by impact related bright frosts in very young bright ray craters (e.g., Osiris on Ganymede), and the absence of concentric and radial fractures surrounding the dome, which would form if intrusion occurred after the impact site had cooled.

For domes to have such a different morphologic expression from the surrounding massif ring and crater floor suggests that the uplifted material is rheologically different from near-surface materials. Fracture networks on these domes resemble those formed in a thin chilled crust over plastic material deforming under gravity (e.g., pancake domes on Venus;

McKenzie *et al.* 1992). This suggests that uplifted dome material deformed plastically during or after emplacement, as would be expected for warm material rapidly uplifted several kilometers and left to cool to space. Dome profiles can be used to model the rheology of the uplifted material during emplacement. Schenk (1993) estimated viscosities on the order of 10^{16} Pa s, and yield strengths of several tens of kPa, using simple Bingham rheologies. While these estimates are consistent with warm ice, the applicability of such models to impact disrupted material is uncertain as emplacement times are unknown. Future high resolution images of the most recently formed domes, particularly Tros and Osiris on Ganymede, would be most valuable in establishing formation conditions and mechanisms. Also, the persistently higher albedo of central domes over time implies an inherent compositional difference with material uplifted from several kilometers being more ice-rich than near-surface materials on both Ganymede and Callisto.

18.3.4 Origin of Pedestals

Annular plateaus or pedestals surround many impact craters on Ganymede and Callisto (see Figure 18.10 for examples). These deposits resemble a subset of unusual ejecta deposits on Mars; i.e., rampart ejecta (see Barlow *et al.* 2000), the potential implication being that ice was also present on Mars (e.g., Stewart *et al.* 2001). General mapping of ejecta deposits on Ganymede (Schenk and Ridolfi 2002) reveals two major ejecta units; the inner or pedestal facies D_p, (e.g., Horner and Greeley 1982), and the outer or radial ejecta facies (D_e), equivalent to the maximum extent of the continuous ejecta deposit as a whole. Both units have a well-defined dimensional relationship to crater diameter (Schenk and Ridolfi 2002),

$$D_e = 4.03D^{0.086} \tag{18.1}$$

$$D_p = 2.44D^{0.91} \tag{18.2}$$

forming the basis of rim-ejecta scaling arguments used earlier in this chapter to predict rim diameters. Pedestal facies are often associated with units of different albedo or color (bright on Ganymede and Callisto, dark and reddish on Europa (Schenk and Ridolfi 2002, Moore *et al.* 1998, 2001)), but the outer facies of continuous ejecta rarely display albedo or color much different from surrounding terrains.

Ideas for pedestal origins include radial flow or plastic deformation of the thicker inner portion of the ejecta deposit (e.g., Horner and Greeley 1982, Moore *et al.* 1998), forming a convex snout (in profile) as flow or creep halted. Higher resolution images of seemingly smooth-edged pedestals reveals that this topographic margin is commonly fluted or gouged (e.g., Schenk and Ridolfi 2002). If plastic deformation is involved in pedestal formation, then the ice must be relatively warm (Moore *et al.* 1998) or interbedded with melt deposits which would enhance slip or creep. High-resolution (50 m/pixel) imaging of the ejecta deposit of Manannán on Europa reveals multiple overlapping flow-like deposits within the crater and on the pedestal deposit radiating from crater center (Moore *et al.* 2001). These could be glacier-like plastic flows of impact debris or flows of impact melt draped over the primary ejecta deposit. Although pedestal deposits could be related to the nature of ice on these surfaces, other flow-like ejecta deposits found on Mars, including lobate ejecta, have not been observed at high resolution on the Galilean satellites. Nor have pedestal deposits been observed on other icy satellites (pending *Cassini* high-resolution imaging), possibly due to colder and thicker lithospheres, and thus less easily mobilized, on these satellites. A search for flow-like ejecta on Titan will provide an interesting test of these models. Thus the relationship of pedestal deposits on icy satellites to unusual ejecta on Mars remains tentative.

18.3.5 Origin of Palimpsests

Palimpsests and other related impact features present a persistent conundrum in that it is not obvious how to map the original rim diameter. Determination of the effective crater diameter is necessary not only to explain the bright deposit, but also to map out the size–frequency of these ancient impact features given that proposed interpretations encompass more than a factor of two in possible diameter. That palimpsests are impact features is not really in doubt. Three basic impact models have been proposed to explain the nature of the bright material and the location of the original crater rim: (1) a crater floor deposit with the crater rim lying near the outer bright margin (Hartmann 1984), (2) the inner or pedestal ejecta facies, with the rim interior to the bright margin (Schenk 1996, Schenk and Moore, in preparation), or (3) the outer or continuous ejecta facies, with the crater rim located even further interior (Shoemaker *et al.* 1982, Jones *et al.* 2003).

Thomas and Squyres (1990) proposed that the bright material was essentially a volcanic outflow from the crater center triggered by impact through the lithosphere into a shallowly buried convecting layer composed of very warm low viscosity ice. In this model, for circularity to be achieved on rugged dark terrain (e.g., Prockter *et al.* 1998a) and, more importantly, for any regularity in the rim to outer-margin ratio to be maintained (especially for penepalimpsests), the extrusion would have to be fairly rapid and part of the excavation process.

High-resolution images of Memphis Facula, Ganymede (the only true palimpsest so observed by *Galileo*), reveal a degraded surface in which local-scale geomorphic units such as ejecta are obscured or unmappable. In broad form, penepalimpsests resemble palimpsests (Figures 18.1, 18.5, 18.7; see above) and are interpreted as transitional between palimpsests and dome craters. Shoemaker *et al.* (1982) equated the central smooth zones of palimpsests with the crater floor, but central smooth areas in penepalimpsests, as discussed above, can be shown from scaling arguments to be dimensionally equivalent to central domes of larger central dome craters. By extension, the outer portion of the bright albedo patch that constitutes palimpsests also corresponds to the inner pedestal ejecta facies (Schenk and Moore, in preparation), rather than the outer limit of continuous ejecta as argued by Jones *et al.* (2003).

Equating palimpsest bright material with pedestal ejecta is consistent with what is known about impact crater ejecta (Horner and Greeley 1982, Chapman and McKinnon 1986, Melosh 1989, Schenk and Ridolfi 2002). Continuous ejecta materials feather out to negligible thickness at the distal margin and are usually partly mixed into the orig-

inal surface, and thus less likely to be preserved over time against degradation processes inherent to dark terrains (e.g., Prockter *et al.* 1998a). With the possible exception of dark halo craters on Ganymede (Schenk and McKinnon 1985), the outer ejecta unit is not generally preserved as an albedo feature on these satellites, and does not form a raised morphologic feature in any craters in the solar system. (The morphometry of dark halos in Uruk Sulcus, Ganymede (Figure 4 in Schenk and McKinnon 1985) is intermediate to that of pedestals and continuous ejecta (Eq. 18.1 and 18.2), but merges with that of continuous ejecta at large sizes.)

On the other hand, inner pedestal ejecta deposits are thicker and often have steeper outer margins and a relatively high albedo, as do penepalimpsest and palimpsest margins (except on Europa wherethey are darker than surrounding terrains (Moore *et al.* 1998, 2001)). Pedestals are the major ejecta-related feature most commonly preserved in older craters. Further, the size and distribution of mature craters with dark floors and dark continuous ejecta deposits can be used to map the thickness of strata with different albedos (e.g., Hawke and Bell 1981), such as for bright terrain on Ganymede (Schenk and McKinnon 1985). Here, dark floor and dark ejecta (i.e., dark halo) craters are common along the periphery but absent in the central portions of palimpsests such as Memphis Facula. This implies that the bright material forming palimpsests is relatively thick towards the center but thinner along the margins (Shoemaker *et al.* 1982, Thomas and Squyres 1990). Thus the evidence for a thicker deposit near the center, and preservation of an albedo feature and a topographic step along the outer edge is entirely consistent with the interpretation of palimpsest (and penepalimpsest) bright material as crater floor material and the relatively thick pedestal ejecta deposit.

The lack of topography across palimpsests requires explanation. The overall similarity between palimpsests and penepalimpsests suggests that palimpsests could be highly viscously relaxed versions of penepalimpsests. Alternatively, the concentric features characteristic of penepalimpsests may have collapsed more rapidly or may not have formed as fully during the impact process due to impact into a lithosphere that was inherently weaker than at the time of penepalimpsest formation (e.g., Greeley *et al.* 1982, Turtle and Ivanov 2002, Schenk 2002). This weakness might be due to significant amounts of fluid in the target (Greeley *et al.* 1982). A weak lithosphere might discourage formation of topographic features such as rim walls or central massif rings. Whatever the basic mechanism, palimpsests would seem to argue for a higher heat flow in the period shortly before bright terrain formation (e.g., Passey and Shoemaker 1982). Formation of penepalimpsests during and shortly after bright terrain formation would argue for a decreased heat flow and an enhanced ability of the lithosphere to form or support topographic features. Here again, more realistic modeling of cratering in icy lithospheres is required before we can fully solve the riddle of palimpsests.

18.3.6 Intersatellite Comparisons and Internal Structure

The similarity in simple crater depths on the Galilean satellites and the Moon suggests that the basic crater excavation process in the gravity regime is to first order indistinguishable on icy and rocky planets. Other details may emerge once we acquire meter-scale images of fresh simple craters on these satellites from some future mission. Complex craters present a different story. The crater modification process is influenced by factors such as gravity (being similar on the Moon and all three icy Galilean satellites) and material properties (e.g., Melosh 1989). As described above, three breaks in slope occur on depth/diameter curves on the Galilean satellites, in contrast to two on the terrestrial planets. The first break in slope, Transition I from simple to complex morphology, is similar on all three satellites (2–4 km) but smaller than on the Moon (Figure 18.2), as are the depths of complex craters. Pike (1980) proposed that simple-to-complex transition diameters for the planets scale inversely with gravity. Schenk (1991) further argued that the icy satellites followed a similar trend by offset to much smaller diameters than on the silicate planets. The basis for this relationship is not firmly established but is most likely related to $c/\rho g h$, where c is a transient material strength, ρ is the surface density, and h is the crater depth at the transition diameter (e.g., Melosh 1989, Melosh and Ivanov 1999).

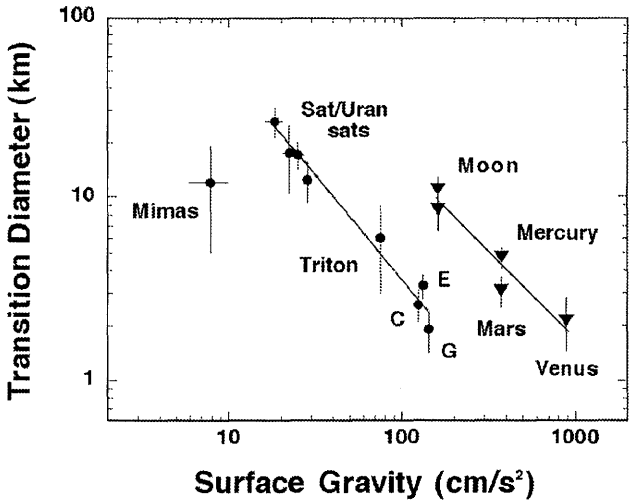

Figure 18.12. Simple-to-complex transition diameters for silicate planets (triangles) and icy satellites (dots). Data from Pike (1980, 1988), Croft *et al.* (1995), Schenk (1991, 2002). Lunar transitions are shown for mare (bottom) and highlands (top). Saturnian and uranian satellites (Sat/Uran sats) include Tethys, Rhea, Dione and Ariel. Callisto, Europa, and Ganymede (CEG) are also shown. Inverse correlation between transition diameter and surface gravity is apparent for each type of body, with icy satellites offset toward lower transition diameters. Only Mimas (and possibly Miranda, not shown) are exceptions to the inverse correlation trend for icy satellites.

The revised estimates for Transition I on Ganymede, Callisto, and Europa strengthen the case for an inverse relationship between surface gravity and simple-to-complex transition for all the major icy satellites of Jupiter, Saturn, and Uranus, with the exception of Mimas (Figure 18.12). H_2O and other ices are inherently weaker (plausibly implying a lower c) than most silicates and this is probably reflected in the offset lines in Figure 18.12, but other factors controlling this transient impact strength could include surface melting point, or local thermal conditions. Ther-

mal properties may be especially important when comparing larger craters on Europa with those on Ganymede and Callisto, an aspect we will explore next.

Depth/diameter (d/D) trends for larger complex craters on all three icy satellites (Schenk 2002) are characterized by rollovers not seen on any terrestrial planet (Figure 18.2). Of particular relevance are the two pronounced breaks in the d/D trends at which depths begin to decrease rather than increase with diameter, representing a deviation from the normally increasing complex crater d/D trends on the terrestrial planets. Lunar basins show a continuous increase in depth up to ~12 km for the largest known basins (Williams and Zuber 1998), whereas no crater or basin on Ganymede exceeds 2 km depth (Figure 18.2). Transition II represents the first change from normally increasing complex crater depths to constant or slightly decreasing depths. On Ganymede and Callisto, this transition correlates with the change from central peak to central pit and central dome morphologies; on Europa this transition correlates with the progressive degradation of central peak and crater rim morphologies. For comparison, Transition II on the Moon correlates roughly with the onset of peak ring basin formation.

Transition III is characterized by major reductions in crater depth (Figure 18.2) and by the development of even less classical impact morphologies (Schenk 2002). On Ganymede and Callisto this is the transition from central dome to anomalous dome, penepalimpsest, or palimpsest morphology, depending on age. We have described above how Transition III may have changed with time on Ganymede (and possibly Callisto), from roughly 60 km in the period following bright terrain formation to >150 km today. On Europa, Transition III correlates with the relatively abrupt change from central peak craters (e.g., Pwyll, 27 km) to multi-ring impact features (e.g., Callenish, 33 km) over a narrow crater diameter range of several kilometers. Both Transition II and Transition III are 3–5 times smaller on Europa than on Ganymede or Callisto (Figure 18.2).

In the simplest explanation, these differences in morphology and depth/diameter statistics record fundamental differences or changes in the thermal profiles of the three satellites (Schenk 2002), either in the history of individual satellites or on Europa relative to Ganymede and Callisto. On Ganymede and Callisto, this is most obvious in the change over time (Figure 18.1) from palimpsest to penepalimpsest to anomalous dome and finally to central dome morphologies in larger craters (>60 km across), and also in the apparent change in diameter for Transition III. As discussed above, viscous relaxation is unlikely to directly produce the anomalous landforms associated with Transition III. Rather, these changes are interpreted as due to lesser or greater degrees of collapse during formation, due to variations in target properties. In this scenario, variations in heat flow and hence ice rheology are the strongest candidates for controlling the degree of collapse and final morphology of craters on large icy satellites (e.g., Turtle and Ivanov 2002, Schenk 2002). Hence, thermally controlled variations in the degree of prompt floor and rim collapse, involving part or all of the lithosphere or parts of the asthenosphere could lead to highly non lunar-like impact morphologies, but a fully realistic model of impact crater modification and icy lithospheric structure does not as yet exist.

If impact collapse and morphology is related to thermal state, as argued here, then the change from palimpsest and penepalimpsest morphology to dome crater morphologies around the time of bright terrain formation appears to mark a major transition in Ganymede's thermal history. The same may be true for Callisto but there is no global resurfacing unit with which to correlate changes in crater morphology. Assuming linear lithospheric thermal profiles, which may or may not be realistic, Schenk (2002) suggested that the smaller transition diameters on Europa implied a heat flow 3–4 times higher and thermal lithosphere proportionally thinner than either Ganymede or Callisto. The change from ~60 to ~150 km for Transition III on Ganymede (and possibly Callisto) suggests that heat flow was considerably higher in the past on these two satellites (Schenk 2002). These transitions are less precisely defined due to the overlapping cratering record, but the factor of ~2 or more increase in Transition III suggests that heat flow on Ganymede at least has decreased by a factor of 2 or more (or lithospheric thickness has doubled) from the time of bright terrain formation. Obviously, detailed thermal models using more realistic thermal profiles should give us more robust estimates of lithospheric thickness, at least in a comparative sense.

The smaller number of palimpsests on Callisto (8 as compared to 37 on dark terrain, which covers only 34% of Ganymede) poses a challenge. (The "palimpsests" in the interiors of the large multi-ring features Adlinda, Asgard and Valhalla are not considered true palimpsests because of the rugged rings formed with them and also because they are much smaller with respect to the original crater rim. Rather, these are interpreted as bright floor deposits.) If palimpsest formation on Ganymede is related to warmer thermal profiles in earlier times, the presence or lack of palimpsests on Callisto may help determine the timing and vigor of heat flow in its early history. The heavier cratering history and unusual landform degradation processes on Callisto (Chapter 17, Figure 17.22) may have obscured or erased some palimpsests, however. The only palimpsest on Callisto observed at high resolution (15° N, 350° W; Figure 5 in Schenk 1995) appears to have been eroded into innumerable knobs (Chapter 17), suggesting that palimpsests on Callisto may be subject to erosion processes not prevalent on Ganymede. Most palimpsests and candidate palimpsests on Callisto were observed under poorer resolution or illumination conditions than on Ganymede, however, and some could be penepalimpsests.

Given the similarities in surface gravity, systematic changes in crater morphology and shape with age most likely record differences in internal properties between the satellites and over time on a given satellite. Large impact structures are thus potentially important probes of satellite interiors. For example, the identical shapes and morphologies of large craters on Ganymede and Callisto suggest that the upper tens of kilometers of Callisto are equally ice rich (Schenk 2002), otherwise crater depths and morphologies would be more similar to those on the terrestrial planets. Thus the outermost portions of Callisto are probably differentiated into water ice as suggested by gravity interpretations (McKinnon 1997, Anderson *et al.* 2001).

18.3.7 Europa's Putative Ocean

The situation on Europa is much different than on its sister icy Galilean satellites (Schenk 2002), with the transition to anomalously shallow craters occurring at smaller diameters (~8 km) than on Ganymede and Callisto (~30 km). This correlates with a progressive degradation of complex crater morphologies, leading to the disappearance of any crater form on Europa at diameters >30 km, and replacement with multi-ring impact morphologies (such morphologies and implied thermal conditions occur on Ganymede or Callisto only at larger diameters and in ancient times). As the outer layers of these satellites are now known to be mostly water ice (see Chapters 13, 15, 16 and 17), the 3–5 times smaller transition diameters on Europa point to thermal gradients that are much higher and a lithosphere that is thinner on Europa.

The unusual multi-ring impact morphologies on Europa (Figure 18.10) may be related to impact into an ice shell at least 10 km thick over water (Moore *et al.* 2001). Multi-ring formation theory on icy satellites (McKinnon and Melosh 1980, Melosh 1989) argues that large impacts into a thin icy lithosphere over an icy asthenosphere that is or can behave as fluid will produce a series of concentric extension fractures and a flattened crater floor. Whether the underlying material controlling the formation of features such as Tyre or Callanish on Europa (or multi-ring features on Ganymede and Callisto for that matter) was truly liquid is difficult to determine. The abruptness of the transition from complex craters to multi-ring features on Europa and the lack of any true crater landform at the heart of these features argue for a similarly abrupt transition at depth, solid to liquid water being a logical candidate. The lack of topography within these craters is suggestive of very warm temperatures at depth, and perhaps the transition from ice to water is shallow indeed.

Whether multi-ring features truly demonstrate the existence of Europa's ocean (e.g., Moore *et al.* 1998, 2001, Schenk 2002) remains to be tested, but the observed depth/diameter transitions place important constraints on ice shell thickness. The presence of central peaks on the short side of Transition III implies the presence of a coherent crust beneath these craters. Modeling of impact melt production by Turtle and Pierazzo (2001) indicates an absolute minimum thickness of 3–4 km. Numerical modeling of europan craters by Turtle and Ivanov (2002) suggests that liquid water may be at relatively shallow depths (approximately one transient crater diameter) beneath anomalous craters, but additional work is required, as the impact process is still only partially understood. Although uncertain to ~10–20%, the transition at $D \sim 30$ km defined by the change from complex craters to multi-ring features on Europa translates into a minimum shell thickness and depth to liquid water of at least 19 km (Schenk 2002).

If Transition III is a detection of Europa's subsurface ocean, what about the same transitions on Ganymede and Callisto? The apparent detection of oceans within both satellites (Zimmer *et al.* 2000, Kivelson *et al.* 2002) at inferred depths of 100–200 km depths came as a surprise, but these depths are uncertain to 50% or more. Transition III on these satellites (Fig. 18.2) was interpreted to indicate lithospheric transitions at depths of 80–100 km presently, but 35–45 km deep around the time of bright terrain formation (Schenk 2002). These depths could be detections of subsurface layers or liquid-rich zones on these satellites, but unfortunately, the physics of the multi-ring problem is too poorly understood to be sure.

18.4 CRATER SIZE DISTRIBUTIONS

The changes in thermal history described above may be related to resurfacing events and orbital dynamics (e.g., Showman and Malhotra 1997) but we have deferred a discussion of the critical subject of when these changes may have occurred. Before reviewing competing models for surface ages, we describe the actual crater populations on the icy Galilean satellites, on which there is general agreement (Chapman *et al.* 1998, Bierhaus *et al.* 2000, Neukum *et al.* 1998, 1999). Until the late 1990s, what was known about crater size distributions on the Galilean satellites was based on imaging obtained during the two *Voyager* flybys (Chapman and McKinnon 1986). Imaging by *Galileo* has greatly augmented and in some ways changed our perception of this population. In particular, the combination of much higher resolution, higher quality CCD imaging and the ability in a multi-flyby mission to select sequences with good lighting and geometry has helped to define crater populations to much smaller sizes, down to less than 100 m diameter in limited areas on all three satellites. Effective completion by *Galileo* of global imaging down to ~3 km/pixel or better resolution over 90% or more of the surfaces of Ganymede and Callisto has permitted global mapping of craters of all sizes down to ~10 km diameter and allows for a global search for more degraded craters. Europa received special attention during the extended mission because of its inherent scientific interest and intriguing discoveries early in *Galileo*'s nominal mission.

As with crater morphology, *Galileo*'s advances were compromised somewhat by the low data rate occasioned by failure of the high-gain antenna to deploy. Areal coverage of Europa at all resolutions is particularly uneven. Nor was it possible to obtain high quality coverage at all longitudes of each satellite, limiting definitive studies of leading/trailing side differences. Areal coverage of Callisto at medium resolution (<1 km/pixel) and low-sun images of Ganymede at higher resolution are less than completely satisfying. And it was only late in the extended phases of the mission that limited, very high resolution images were taken of Ganymede and Callisto. In a few cases, it was also impossible to precisely register these very high resolution images on the surface of Callisto. It is presently uncertain to what extent the limited high-resolution samplings are compromised by local geology and how representative of the smallest craters they are of the general population.

The primary issues raised by crater size distributions include: (a) What is (and has been) the cratering production function (i.e., the size distribution of the impactor populations) and how does it differ from that expressed in the more thoroughly studied cases of Mars and the Moon? (b) What can be said about processes that degrade craters: how do they degrade craters of various sizes, are the processes active only in certain regions on a satellite, and are they specific to particular satellites or operative on all three of the icy satel-

lites? (c) What processes, other than primary cratering by hypervelocity projectiles in heliocentric orbits, create craters or pits on the satellite surfaces (secondary cratering, circumjovian projectiles, endogenic cratering)? (d) How long have different units been exposed to impact cratering (i.e., what is the crater retention age of the surface)?

Voyager revealed no craters on Io, and the much higher resolution *Galileo* imaging also has failed to reveal an unambiguous ionian impact crater. Although circular dark spots are not uncommon, they are of similar dimensions and brightness as oval dark spots of obvious volcanic origin (see Chapter 14). *Voyager* views of Europa revealed very few craters. Rounded depressions observed early on by *Galileo* are now seen, at higher resolutions, to be endogenic "pits" (formed by collapse or disruption of the surface, or by visual misperception of intersecting linear ridge sets) although several large features seen as dark spots or concentric patterns in *Voyager* images are now resolved as impact features. The primary *Voyager* focus was on the more heavily cratered satellites Ganymede and Callisto. Although there were dissenters, many researchers (e.g., Strom *et al.* 1981) viewed the Ganymede/Callisto crater distributions as being distinctly different from terrestrial planet populations in at least two respects. First, there appeared to be a remarkable scarcity of very large craters (>100 km diameter), especially on Callisto (Woronow *et al.* 1982), but these counts did not include some large multi-ring or any degraded impact features such as palimpsests. Second, the shape of the size distribution at smaller sizes (e.g., 15–50 km diameter) appeared to be "steeper" than the −2.3 slope for the differential log–log power-law size distribution for lunar highlands craters over that size range.

18.4.1 Ganymede and Callisto

Galileo data have clarified the nature of the crater size distributions on all three icy satellites at both small and large diameters. The data are presented as R-plots, which can be thought of as normalized differential plots where the D^{-3} power-law slope, which would plot as a horizontal line, has been "removed." This allows us to examine the structure of the size–frequency distribution with greater clarity. For comparison purposes, the global counts are also shown as cumulative plots.

With our improved understanding of large impact morphology on these satellites (see above sections), including palimpsests and multi-ring structures, it is now possible to include these in the global crater counts. The revised production population for Callisto (Figure 18.13, Table 18.1) has a cumulative slope of only −2.3 between 50 and 1000 km crater diameters (crater counts by P. Schenk) and is not as deficient in impactors that form craters of such sizes as had been thought. There may be a slight turn-up at the largest diameters, but the total number of craters (2) in this size range is very limiting. Given the statistical uncertainties, the population may in fact be relatively flat (log–log slope ~0.1) on an R-plot (Figure 18.14). Counts of two *Galileo* G8 medium resolution imaging (~0.8 km/pixel) sequences near the south pole of Callisto yield similar results for craters between 30 and 200 km across (Figures 18.13, 18.14, Table 18.1).

Crater counts from various units on Callisto in high-

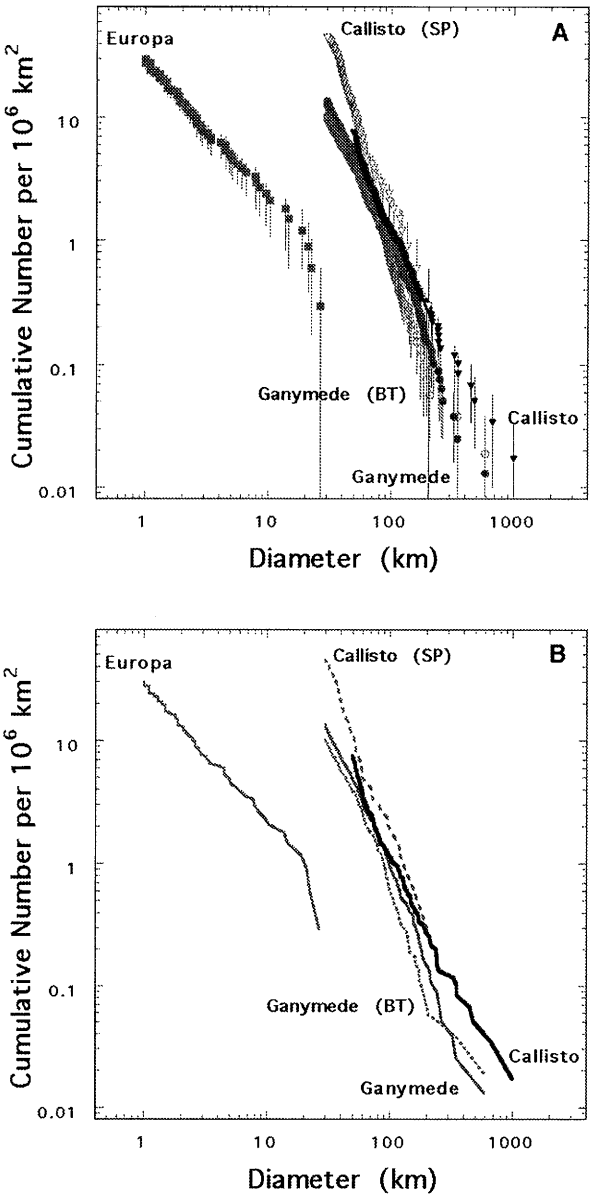

Figure 18.13. Cumulative crater size frequency plots for impact crater densities on the icy Galilean satellites. Plots are shown as raw data (A), and as line plots (B) for clarity. Shown are global data compilations for large craters on Callisto ($D > 50$ km), and Ganymede ($D > 30$ km), as well as plots for bright terrain on Ganymede (Ganymede BT), and the *Galileo* C8 south polar observation described in the text (Callisto SP). A global count of craters larger than 1 km on Europa is also shown. Note the shallower slope for europan craters, although the Europa data are for craters smaller than those plotted here for Ganymede or Callisto (see also Figure 18.14).

resolution *Galileo* images (counts by Bierhaus *et al.* 2000) indicate a differential slope of −2.5 on average over the range 0.5 to 20 km diameter (Figure 18.14, Table 18.1). This is distinctly steeper at diameters larger than 10 km than for similar size distributions on the Moon, Mars, and Mercury. A turn-up to steeper slopes at 0.5 km and smaller diameters is indicated in a couple of locales, but with an onset

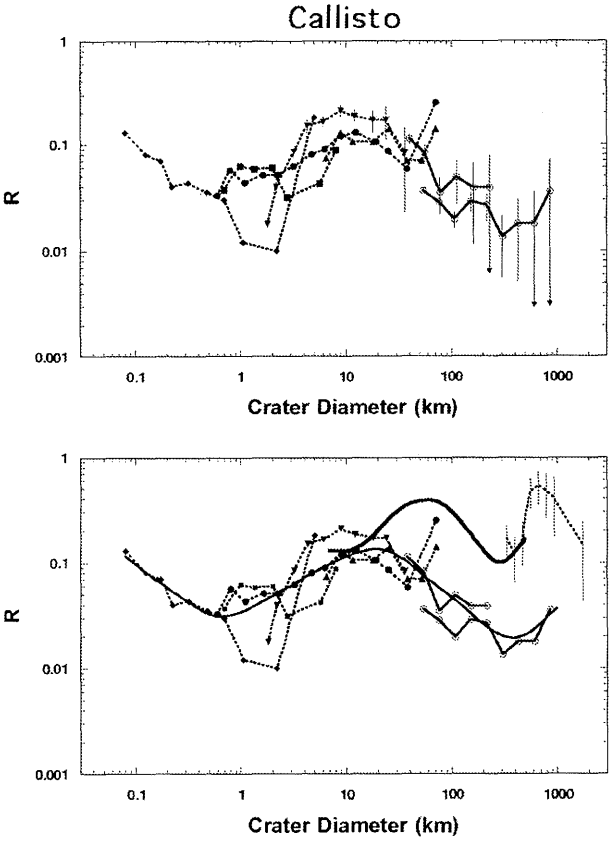

Figure 18.14. *R*-plots of impact crater densities on Callisto. (Top) Shown are counts for *Galileo* high resolution observations of Callisto (dashed curves with closed symbols), and the global counts down to 50 km diameters described in text (solid curves with open symbols; see also Figure 18.13). Representative error bars are shown for several observations. (Bottom) Original counts are shown in comparison to lunar highlands crater densities from Ivanov *et al.* (2002) (heavy curve) and from a count of large basins >300 km across as revealed by *Clementine* altimetry (data from P. Spudis, personal commumication, dashed curve with error bars). The thin curve without error bars is a modeled representation of the currently available Callisto data (see Table 18.1).

at much smaller sizes than is evident on the Moon (about 8 km, Ivanov *et al.* 2002). There are clearly variations in the population from site to site, but stochastic variations in cratering or erasure are not unexpected.

It is clear from the diverse samples represented in Figure 18.14 that Callisto's revised global crater population differs from the lunar population (Table 18.1). The overall crater density on Callisto is on average several factors lower than on the lunar highlands. In a relative sense, Callisto's crater population decreases from ~20 km to ~450 km. There may be a turn-up at the largest diameters but the number of such craters is small and statistics poor. Regardless, there is no spike in 400-km diameter and larger craters as is now apparent for the Moon. Relative crater density again decreases shortward of 20 km. The turn-up to higher crater densities occurs at much small diameters on Callisto (below ~1 km) than on the lunar highlands. Although in this case based on counts from only 1 site, additional very high resolution images appear to show roughly similar crater densities.

Although the visual appearances of the surfaces of Ganymede and Callisto in the highest resolution samplings (e.g., the G28 BRTDRK01 sequence and C30 HIRES_02 sequence, respectively) differ enormously (Chapter 17), counts of craters in the 100 to 500 m size range are roughly the same to within plausible systematic errors (counts by B. Bierhaus). Since the spatial densities are below $R = 0.1$, these crater populations do not reflect saturation equilibrium, as may be true for craters of such sizes on the Moon. Since the small craters on both satellites show a range of morphologies, from fresh to highly degraded, their numbers presumably reflect a balance between creation (whether by heliocentric, planetocentric, or secondary ejecta impactors) and erasure by comparatively recent, active, erosional processes (e.g., sublimation degradation).

18.4.2 Europa

Sparsely cratered Europa presents a very different case from its sibling icy satellites. Only about 24 craters ≥10 km diameter are known on Europa, a number that is certainly incomplete due to highly variable longitudinal image coverage. Clearly, the average crater-retention age of its surface is far too low to have retained a statistically significant sampling of the impactor populations that create large craters. Hence Europa sheds no light on the population of such larger craters and we must presume that the production function is the same as expressed on Ganymede and Callisto.

Two types of counts have been done to date for Europa. Small crater statistics have been compiled by B. Bierhaus (Bierhaus *et al.* 2001a, 2001b) on low-sun high-resolution (<100 m/pixel) *Galileo* images, including craters down to ~50 m diameter. These images include few if any 1-km and larger size craters, however. To obtain a "clean" global sample of the larger crater population unbiased by variations in illumination or the factor of >15 global variation in resolution, craters were counted on low-sun images between 180 and 300 m/pixel (counts by P. Schenk), covering ~11% of the surface. These include the E11, E15, and E17 REGMAP observations, among others, and allow counts down to ~1 km diameter (imaging at >65° emission angles were excluded), but exclude those areas surrounding large primary craters such as Callanish due to the large concentrations of secondary craters. There are additional large craters visible in low resolution or high-sun images, but these are not included as they would bias the global survey toward large craters. A few impact crater clusters were observed in the global survey but they were not included as these were deemed obvious secondaries (Bierhaus *et al.* 2001).

At sizes around 1 km and larger, craters on Europa are extremely rare, down hundreds of times from empirical saturation densities, resulting in typical moderate-resolution frames (pixels a few hundred meters across) showing only a handful of craters at most. Nevertheless they are abundant enough to represent a sampling of the production function on Europa. The "global" large crater counts (1- to 25-km diameters) show a much less steep cumulative slope, −1.2, than do global counts of Ganymede and Callisto (Figures 18.13, 18.15, Table 18.1). There may be a steepening of the distribution at ~20 km diameters, but there are too few craters in the counting area to be sure. In this size range,

Table 18.1. Crater size–frequency distributions for the icy Galilean satellites.

Satellite	Diameter Range (km)	Area (10^6 km^2)	N	Cumulative Slope*	Differential Slope*
Europa					
- global	1–30	3.9	126	−1.16	−2.04
Ganymede					
- global	30–600	78.5	1059	−2.21	
- global	30–85	78.5	934	−2.01	
-	85–300	78.5	122	−2.70	
-	300–600	78.5	3	−1.64	
- bright terrain global	30–600	52.3	539	−2.26	−3.58
-	30–85	52.3	476	−1.98	
-	85–300	52.3	61	−3.16	
-	300–600	52.3	2	−1.36	
- C9 bright terrain	10–155	0.7	47	−1.45	−2.00
- Gilgamesh	3.5–23	0.3	29	−1.57	−2.24
Callisto					
- global	50–1000	59.6	446	−2.26	−3.12
- global (model *R*-plot)	0.08–0.5	N/A	N/A	N/A	−3.74
-	0.5–20	N/A	N/A	N/A	−2.50
-	20–430	N/A	N/A	N/A	−3.71
-	430–1000	N/A	N/A	N/A	−2.00
- G8 southern	30–200	3.4	153	−2.77	−3.58
- Lofn	3.5–34	0.3	29	−1.23	−1.92
- Valhalla	10–85	2.1	87	−1.79	−2.25

* Unweighted fits.

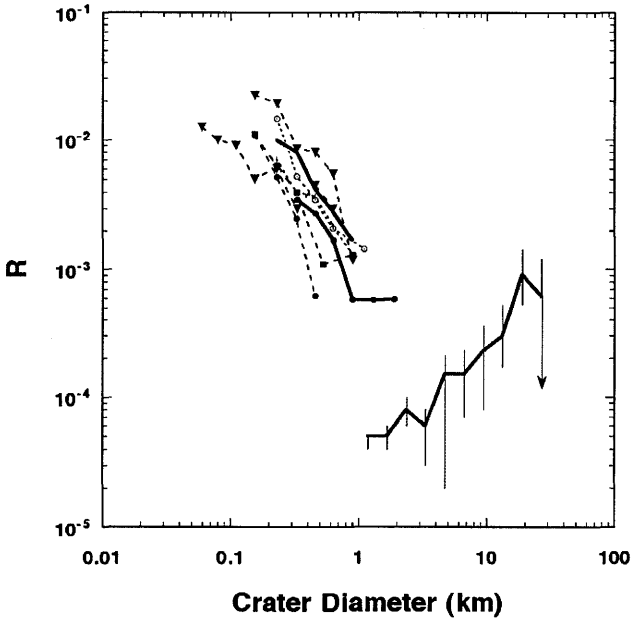

Figure 18.15. *R*-plot of impact crater densities on Europa. Shown are counts for *Galileo* high resolution observations of Europa (dashed curves with symbols), and the global counts down to 1 km diameters described in text (solid curve with open symbols; see also Figure 18.13).

the size distribution for Europa is rather similar to that on young basins on Ganymede and Callisto (Figure 18.16).

Starting at about 1-km diameter and smaller, however, most regions on Europa show a sharp increase in the relative numbers of smaller craters (Figure 18.15). Although small crater densities vary regionally by a factor of 20 or more, nearly all small crater populations, down to the smallest sizes resolvable in the highest resolution images, show a very steeply sloping differential power-law index, typically −4 or even steeper (Figure 18.15). The steep differential slope, characteristic of secondary crater populations, suggests that most small craters are not primary craters but rather secondaries from the few large 10–50 km primaries. This hypothesis is strengthened by the demonstration (Bierhaus *et al.* 2001) that well over 80% of small europan craters occur in spatial clusters, which are sometimes associated with visible rays from craters like Pwyll. Given the apparent likelihood that most small craters are secondaries, the shape of the production function for primary craters <1 km must be comparatively shallow, indeed shallower than that expressed on asteroids like Gaspra and on the terrestrial planets. Bierhaus *et al.* (2001) have also demonstrated that the few large primary craters on Europa are sufficient to produce all of the smaller craters from secondary ejecta, so it is not necessary to invoke any small primary impactors.

In summary, the Europa size–frequency distribution resembles an asymmetric "V" (on an *R*-plot) with two upward wings (Figure 18.15). The wing at smaller diameters is dominated by secondary craters, the large diameter wing by primary craters. Whether the apparent steepening of the cumulative distribution at diameters larger than ∼20 km (Figure 18.13) is real or reflects a similar change observed at Ganymede and Callisto must await a global mapping mission at Europa.

With respect to the bottom of the "V", several explanations are possible for the apparent difference in crater densities at ∼1 km diameter between the global survey results and the high resolution counts (Figure 18.15). The likelihood that the eight high resolution sites are all atypical of Europa at large is low but not negligible. It is more likely, however,

that the global survey is incomplete at these diameters. One reason may be the sampling strategy for the global survey, which rejected clustered impacts as due to secondary cratering. Alternatively, the intensely ridged nature of the surface may render 1–3 km diameter craters difficult to detect (the counts are considered complete at 3 km and larger). The fact that we were limited by imaging constraints to a counting area of only ~11% of the surface leaves us with an incomplete record of Europa's cratering. Global imaging at ~100 m or better resolution will be required to bridge the gap between Europa's primary and secondary crater populations.

The rather surprising result that most of Europa's small craters are secondaries raises the question about whether the same might be true for similarly sized craters on Ganymede and Callisto; presumably it would be true, at least for the modern era impactor flux. Indeed, if the difference between icy and rocky surfaces is unimportant in ejecta characteristics, there should be a re-examination of the role of secondaries in forming small craters on the Moon and other terrestrial planets. Of course, it is known, independently from crater counts, that there is a comparatively steep size distribution for small asteroids and meteoroids in the inner solar system, which may not be true in the comet-dominated outer solar system. The small-asteroid/meteoroid population in the inner solar system may, nevertheless, be thought of as "interplanetary secondaries," a term invoked by Hartmann (1995) to reflect the origin of many small asteroids and meteoroids from cratering and fragmentation of main-belt asteroids, for which gravity is so low that the ejecta that otherwise would form secondary craters on larger bodies instead goes into heliocentric orbit and becomes part of the "primary" production function. So a potential picture emerges that small crater populations in the inner solar system may be a mixture of heliocentric projectiles of the "interplanetary secondary" sort and, for the Moon and planets, though not smaller asteroids, true secondary craters. Similar intersatellite secondaries could exist in the Jupiter system (see below), but their source would be projectiles launched from larger craters on the satellites themselves and would not be very large (Zahnle *et al.* 2001). And, in the case of the Galilean satellites, small crater populations are dominated by true secondary craters, in part because of an apparent relative scarcity of small comets.

18.4.3 Young Terrains

Young terrains and large young impact basins represent witness plates on which we can potentially map out recent production populations relatively free from secondary populations. This is particularly true for large young basins on Ganymede and Callisto as there are few if any subsequent impacts large enough to produce secondaries of the necessary size. Saturation effects or differential erosion may distort or mask the production function on older terrains on Ganymede and Callisto. Differential resurfacing, secondary cratering and stochastic variations may also confuse the production signature on Ganymede's bright terrains. Crater floor and ejecta units can be considered as having been instantaneously resurfaced. In younger craters these units are also relatively uneroded, and crater populations on these surfaces may give us a clearer picture of the current impactor population. The two large young basins that stand

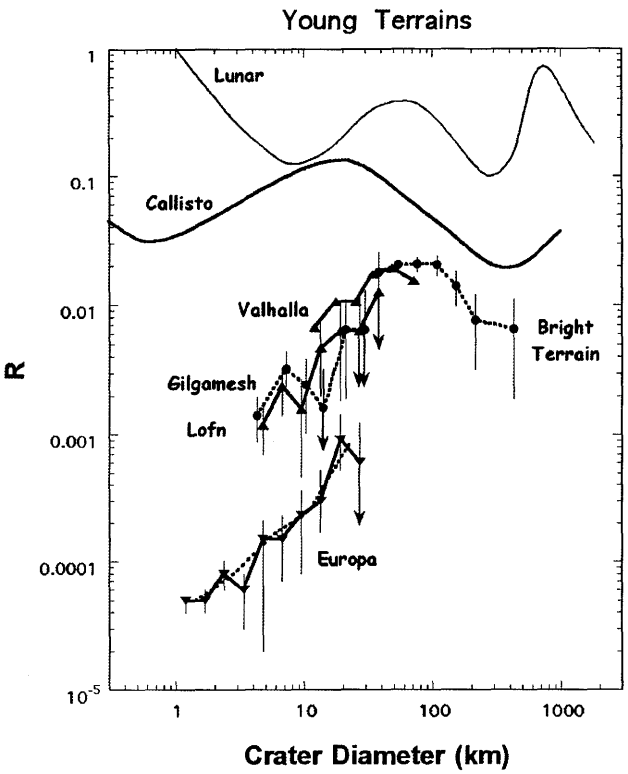

Figure 18.16. *R*-plot of crater densities on relatively young terrains on the icy Galilean satellites. These terrains are inferred to be relatively free from secondary craters from large impact basins, at least at the observed diameters. Plotted are counts for craters superposed on large relatively young impact features Lofn and Valhalla on Callisto (triangles); the young impact feature Gilgamesh and bright terrain on Ganymede (dots), and Europa (inverted triangles). Gilgamesh data have been offset slightly for clarity. Heavy curve (Callisto) is from Figure 18.14, extended to smaller sizes (Ivanov *et al.* 2002). Thin curve (Lunar) is the lunar highlands curve from Figure 18.14. The dashed Europa curve at the bottom represents the Europa data at larger bin dimensions.

out are Gilgamesh (D = 585 km) on Ganymede and Lofn ($D \sim$ 355 km) on Callisto (counts by P. Schenk). Bright terrain on Ganymede may also provide a valuable window into the impactor flux, at least for larger craters, by virtue of its lower crater density and larger surface area.

For Gilgamesh, we work with two counts, one for the feature as a whole and another restricted to its ejecta blanket. The former shows more craters at larger diameters while the latter is more representative at smaller diameters. This clearly shows the difficulty in recognizing small craters in the rugged basin interior, and we use only the ejecta blanket counts here. The rugged interior of Lofn is much less extensive than on Gilgamesh and the counts shown here (Figure 18.16) are taken as representative. Both Gilgamesh and Lofn have relatively shallow slopes, −2.2 and −1.9 (Table 18.1), respectively. Although the surface is somewhat older than Lofn (Wagner *et al.* 1999), Valhalla counts also suggest that there are fewer small craters than expected at smaller diameters. The Valhalla counts are suspect because the surface of the basin is quite rugged and some of *Voyager*'s high resolution images were smeared, reducing the confidence in smaller crater statistics.

Close to 66.6% of Ganymede is covered by relatively young and more lightly cratered bright terrain. We have two samples of bright terrain, the global counts down to 30 km diameter described above, and counts on an 800 m/pixel resolution orbit C9 image strip across Xibalba Sulcus (~70° to 94° W longitude) by P. Schenk down to 10 km diameter. The global survey of Ganymede suggests that crater populations on Ganymede are similar to Callisto at these diameters but fall off at diameters below ~80 km (Figures 18.13 and 18.16). Similarly, the Xibalba Sulcus counts (from 10 to 155 km diameter) indicate a depletion at small diameters, with a differential slope of −2.0 (Table 18.1, not plotted). Taken together with the Europa counts and the large young impact feature counts, we see a generally similar distribution to that observed on ancient terrains of Callisto (Figure 18.16). The exception to this similarity is that the highest relative crater densities are between ~40–90 km diameters on younger terrains, rather than at ~10–30 km as on Callisto (Figure 18.16). This difference could be due to secondary cratering from the 1000-km diameter Valhalla basin or to a real change in the impactor production function (e.g., a depletion in smaller projectiles over time). The cratering production functions are still imprecisely constrained in these diameter ranges due to the limited imaging coverage, however.

For both Ganymede and Callisto, craters with sizes near, and smaller than, the lower limit of *Voyager* resolution have morphologies that have been greatly modified by tectonic and other processes that certainly affect recognizability and preservation of craters, rendering direct comparisons with the production populations in the inner solar system suspect. These processes evidently are different on Ganymede and Callisto; "sublimation degradation" dominates on Callisto but not Ganymede (Chapters 16, 17). In the case of Ganymede, localized albedo effects often further impede recognition of craters. Of course, estimates of production populations from terrestrial planet crater populations, especially Mars, are also affected by processes of crater degradation, including erosion, infilling, and mass wasting due to subsurface ice. We may cautiously conclude, however, that the differences in size distribution between Ganymede/Callisto and the terrestrial planets are far too great for them to have been formed by impactors having the same size distribution. In particular, relative to terrestrial planets, Ganymede/Callisto craters several km in diameter are relatively numerous but craters several hundred meters in diameter are relatively depleted. While the depletions may be due to active modification processes on Ganymede and Callisto, the size distribution differences for several km and larger presumably reflect a different size distribution for the impactors. The preservation of such depletions on relatively young large impact craters also suggests that this is not due primarily to surface modifications but represents a real depletion in small bodies.

18.4.4 Global Asymmetries and Nonsynchronous Rotation

Primary cratering of a synchronously rotating satellite by heliocentric (sun-orbiting) comets or asteroids is expected to be strongly asymmetric, with the leading hemisphere being much more heavily cratered than the trailing hemisphere. Several different analytic formulae for apex–antapex cratering asymmetries have been offered in the literature (Shoemaker and Wolfe 1982, Horedt and Neukum 1984, Zahnle *et al.* 1998). Zahnle *et al.* (2001) revisited this issue using a Monte Carlo model and concluded that the analytical predictions of very large apex–antapex cratering asymmetries are basically correct. The expected effect is that cratering rates at the apex of motion are typically 20–60 times higher than towards the antapex of motion, the precise ratio depending on planet and satellite. It is a notable fact that this apex–antapex asymmetry is almost never seen in the solar system.

Passey and Shoemaker (1982) conducted the first search for apex–antapex asymmetries. They found weak evidence for asymmetry on Callisto but not on Ganymede, although the *Voyager* data lacked coverage over the apex and antapex regions. They used bright rim and bright ray craters, which are not ideal given the sensitivity of detection to solar illumination conditions, differential ray preservation as a function of latitude and longitude, and the uncertain timescales for ray erasure. Schenk and Sobieszczyk (1999) mapped the global distribution of all large craters on both bright and dark terrains on Ganymede and Callisto using combined global image coverage from *Voyager* and *Galileo* (see also Zahnle *et al.* 2001). Only the younger bright terrains of Ganymede exhibit a significant apex–antapex cratering asymmetry. The observed asymmetry is about a factor of 4, which still falls well short of the factor 40 difference predicted for Ganymede. One possible explanation is that we are looking at the effects of crater saturation, in the sense that younger craters are obliterating older craters (Zahnle *et al.* 2001). This seems unlikely given the lower density of large craters on bright terrain. The alternative is dilution of the predicted asymmetric crater record by a more uniformly distributed crater population, the choices being planetocentric debris or nonsynchronous rotation (Zahnle *et al.* 2001).

Planetocentric debris can crater symmetrically (Horedt and Neukum 1984), but there does not appear to be a plausible source for large planetocentric objects in the jovian system. A 30-km diameter crater on Ganymede implies a 2.4-km diameter comet striking at 21 $\mathrm{km\,s^{-1}}$, or a 5-km chunk of planetocentric debris striking at 5 $\mathrm{km\,s^{-1}}$. There are hundreds of 30-km diameter impact craters on Ganymede. It is difficult to put hundreds of 5 km icebergs into orbit about Jupiter (Zahnle *et al.* 2001) (the problem is in creating a dynamically long-lived planetocentric population that can actively crater the satellites).

Our preferred hypothesis is that Ganymede has rotated nonsynchronously some time in the geologically recent past. Nonsynchronous rotation would act to homogenize an asymmetric cratering distribution on a satellite surface over time. In the simplest story the bright terrains would all be roughly the same age, give or take several hundred million years (e.g., Murchie *et al.* 1989), although this is not necessary to preserve the apex–antapex asymmetry (Zahnle *et al.* 2001). What is required to explain the observed weak asymmetry is that about half the big craters on the bright terrains be attributed to a time after synchronous rotation stopped (Zahnle *et al.* 2001). Nonsynchronous rotation implies a warmer mantle and may even require a substantial liquid layer so that the ice shell can effectively decouple from the interior.

The origin of the bright terrains may be related to this time of heating, which in turn may be related to tidal heating driven by a now extinct resonance with Europa and Io (e.g., Malhotra 1991, Showman *et al.* 1997, Chapter 16). Higher heat flows are plausibly reflected in the highly flattened impact crater morphologies of palimpsests and penepalimpsests. This hot period was followed by a slow secular cooling phase, recorded in the change from penepalimpsests to anomalous dome craters to today's central dome craters. Approximately 33% of post-bright terrain craters are anomalous dome craters or penepalimpsests. This was also a protracted period of nonsynchronous rotation, recorded as a uniform crater distribution on bright terrains. After Ganymede became relocked into synchronous rotation at some later time, the currently forming asymmetric crater distribution became mixed with the earlier uniform distribution, creating the weak pattern we see today. If this scenario is correct and we assume that cratering rates were relatively constant over the past several billion years, then the evidence from crater distribution would suggest that Ganymede rotated nonsynchronously for a period extending roughly half way between bright terrain formation and the present. Similarly, if we assume linear cooling rates, then the evidence from cratering morphology would suggest that we did not approach current heat flow values until a time roughly one third from bright terrain formation till the present.

The distribution of catenae, or crater chains, on Ganymede provisionally supports the nonsynchronous hypothesis. As discussed above, the distribution of catenae formed by disrupted comets on Callisto is consistent with formation on a synchronously rotating satellite (Schenk *et al.* 1996). Yet 4 of the 11 known candidate catenae on Ganymede are found on the inaccessible hemisphere, consistent with, but not proof of, Ganymede having rotated nonsynchronously in the geologically recent past (Zahnle *et al.* 2001). Additional photo-geologic study is required to assess the origins of these stray catenae.

Nonsychronous rotation of Europa has been proposed (Greenberg and Weidenschilling 1984), and observationally supported by analyses of lineament orientations (e.g, McEwen 1986, Geissler *et al.* 1998, Chapter 15). Although the crater distribution data are much sparser for Europa (uniform resolution coverage for only ~11% of the surface), the global distribution of 1 km craters on Europa described above shows no evidence of a statistically significant asymmetry, consistent with nonsynchronous rotation in the recent past or ongoing today. Obviously a much better global map of the crater distribution on Europa is required to be confident of this conclusion.

18.5 SURFACE AGES

Lacking samples, efforts to constrain satellite ages have focused on interpreting the cratering record. Although there is general agreement about the nature of observed crater populations on the icy Galilean satellites described above, there is plenty of disagreement about its interpretation. Two opposing approaches have been improvised; unfortunately, the resulting age estimates do not generally converge, and the gentle reader is forced to decide which is most logical. Neukum *et al.* (1998, 1999) and allies essentially work forward from the ancient past, assuming that both the production function and observed heavy cratering record are lunar-like. Shoemaker (Shoemaker and Wolfe 1982), followed by Zahnle (Zahnle *et al.* 1998, Zahnle *et al.* 2003) work backward from the present observable flux of comets. The latter estimates require extrapolating the current population of comets into the distant past. A third wholly independent approach exploits the recent suggestion that jovian stratospheric CO is mostly impact-generated (Bézard *et al.* 2002). This gives the current mass accretion rate of comets by Jupiter but on a short (300 yr) timescale (see Zahnle *et al.* 2003).

18.5.1 A Little History

Neukum and others assume that a single population of impactors was responsible for a solar-system-wide heavy bombardment. Since then cratering has been minimal, at low rates that are consistent with an asteroidal source both in the inner solar system and at Jupiter. They assume that large impact basins such as Valhalla and Gilgamesh were contemporaneous with the large lunar basins Orientale and Imbrium, c. 3.8 billion years ago. The lunar impact rate declined steeply over the next few hundred million years by a factor on the order of 100. As a result, Neukum and his colleagues infer ancient lunar-like ages throughout the jovian system, even for sparsely cratered surfaces like Europa.

By contrast, Shoemaker and Wolfe (1982) argued that comets are much more important than asteroids at Jupiter and beyond. They attempted to constrain the present cratering rate from modern observations of comets. Zahnle and colleagues have reiterated these issues by exploiting the rapidly expanding base of new data (Zahnle *et al.* 1998, 2003). These include new *Galileo* crater counts; revised observational estimates of the numbers of comets near Earth, near Jupiter or seen to strike Jupiter, and near Saturn; and the discovery of the Kuiper Belt as the source of these comets and numerical models that link the Kuiper Belt Objects to comets in the inner solar system (Levison and Duncan 1997).

Jupiter-Family Comets

Most primary impact craters in the outer solar system are currently made by ecliptic comets (Shoemaker *et al.* 1982, Zahnle *et al.* 1998). As the name implies, ecliptic comets are concentrated toward the plane of the ecliptic; i.e., they revolve in prograde orbits that interact strongly with the planets (Levison 1996). They are thought to come from the Kuiper Belt, most likely from its dynamically hotter scattered-disk component (Duncan and Levison 1997). When under Jupiter's control, ecliptic comets are called Jupiter-family comets (JFCs). When between Neptune and Saturn, they are called Centaurs. Ecliptic comets are distinct from the nearly isotropic long period comets and Halley-type comets, which come from the Oort cloud. The nearly isotropic comets do not currently contribute significantly to impact cratering in the outer solar system (Zahnle *et al.* 1998, 2003).

Shoemaker and Wolfe (1982) extrapolated the perihelion distribution of the 80-odd near-Earth short period comets then known to estimate that there are 1400 Jupiter-family comets (JFCs) with diameters $d_c > 0.9$ km. Most of

these would not be near-Earth objects. Therefore, they also constructed synthetic orbits to account for large numbers of undiscovered JFCs with distant perihelia. Because the synthetic orbits are more circular, they generally have higher impact probability with Jupiter, and therefore they tend to dominate the cratering rates. In addition to active comets, Shoemaker and Wolfe also estimated that there are 320 extinct Jupiter-crossing comets. This number is extrapolated from the one such object (Hidalgo) known in 1982. Although Shoemaker and Wolfe do not appear to give this number explicitly, the total impact rate on Jupiter itself by JFCs (active and inactive) would be $\dot{N}(d_c > 2.5 \text{ km}) \approx 2.7 \times 10^{-4}$ per annum.

Levison and Duncan (1997) estimated impact rates on the planets as a byproduct of their numerical simulation of migrating ecliptic comets. They calibrated the total number of JFCs to the number of active comets with perihelia $q < 2$ AU and active absolute magnitudes $H_T < 9$. The latter is usually taken to mean that the comet has a diameter of roughly 2 km; however, the relationship between the size of a comet and how bright it is when active is weak. Moreover, most JFCs are inactive. Several papers have used Levison and Duncan's results to estimate outer solar system impact rates (Zahnle *et al.* 1998, 2003, Levison *et al.* 2000, Bottke *et al.* 2002). Zahnle *et al.* (1998) extrapolated Shoemaker's $N(>d_c) \propto d_c^{-2}$ power law to km-size comets and recommended an impact rate of 0.011 per annum for comets with $d_c > 1$ km, in good agreement with the historical record of comets making close encounters with Jupiter. Levison *et al.* (2000) later revised impact rates on the giant planets downward by a factor of four, recommending an impact rate on Jupiter of $(6.5S) \times 10^{-4}$ per annum with $S = 5$ for km-size comets. The factor S includes uncertainties in the number of inactive comets and uncertainties mapping from brightness to size. Bottke *et al.* (2002) revised the Levison *et al.* (2000) result further downward by using discovery rates of inactive comets in the automated Spacewatch NEO survey. Based on 5 previously unknown asteroids in JFC-like orbits with perihelion $q < 1.3$ AU and $d_c > 1.7$ km (albedo of 0.04), Bottke *et al.*(2002) obtained $S = 1.7 \pm 1.4$. They note that their argument makes the extreme assumption that 100% of JFCs fade rather than disintegrate, and so gives a lower limit. We note that their extrapolation places a heavy weight on the durability of comets that get very near the Sun. In the other direction, Zahnle *et al.* (2003) revise the Levison *et al.* (2000) estimate upward by placing a much heavier emphasis on the historical observations.

Close Encounters and Direct Hits

Six close encounters with Jupiter are known to have occurred in historical times. These were by P/Lexell (2.8 R_J in 1779), P/Brooks 2 (2.0 R_J in 1886), P/Gehrels 3 (3.0 R_J in 1970), and D/Shoemaker–Levy 9 (1.3 R_J in 1992 and 0.5 R_J in 1994). Both P/Brooks 2 and D/Shoemaker–Levy 9 were tidally disrupted into several discrete fragments. The sixth was a spot near the equator observed for two weeks by J. D. Cassini in 1690, as reported by Tabe *et al.* (1997) who show that the observed evolution of Cassini's spot quantitatively and qualitatively agrees with the evolution of a windblown SL9-like impact feature. Tabe *et al.* (1997) rank the 1690 event with the middle-ranking SL9 events, which by our reckoning makes the impactor a 600-m object.

As the distribution of perijove distances of JFCs making close encounters with Jupiter is uniform (the distribution expected in the limit of strong gravitational focusing), we can estimate how frequently Jupiter is hit by exploiting the six close encounters,

$$P_J > \left(\frac{6 \text{ encounters}}{350 \text{ years}}\right)\left(\frac{1\,R_J}{4\,R_J}\right) \approx 5 \times 10^{-3}\text{yr}^{-1} \qquad (18.3)$$

This is conservative because we set the outer distance on close approaches at 4 R_J (although the six known encounters were all well within that distance) and we use the longest possible time line, going back to the first telescopes and observers even capable of seeing such events, and treating them as if they are complete. When this is done more carefully, taking into account the sizes of the comets and the time spans over which they could have discovered, the historical rate is better described as $0.01^{+0.01}_{-0.05}$ per annum for $d_c > 1.5$ km. This point is plotted on Figure 18.17 as "close encounters."

A third independent measure of the current impact rate is provided by carbon monoxide in the jovian stratosphere. SL9 produced $\sim 7 \times 10^{14}$ g of CO from a $\sim 1 \times 10^{15}$ g comet (Chapter 8). The CO was injected at very high altitudes (Lellouch *et al.* 1997). Because CO is nearly inert in the jovian stratosphere, it is only removed by mixing it into the deep troposphere on a characteristic 300-year eddy diffusion timescale (Bézard *et al.* 2003). There appears to be substantially more excess CO in the jovian stratosphere than can be accounted for by SL9 (Bézard *et al.* 2003). If the excess CO is from earlier cometary impacts (Bézard *et al.* 2003), the excess stratospheric CO corresponds to $M \approx 2 \times 10^{15}$ g, implying that the 300-year impact is 1.6 km diameter. The resulting impact rate is 0.003 per annum for $d_c = 1.6$ km (50% higher if we included SL9 itself, as we didn't but perhaps should have). The (mostly stochastic) error associated with this estimate is about a factor of 2 in diameter. This point is plotted on Figure 18.17 as "CO."

The failure of modern observers to detect impact events more often provides an upper limit on the cometary impact rate on Jupiter. Rogers (1996) surveys all observations of Jupiter since 1878, and concludes that "no impact on the scale of SL9 fragments G, K, or L has ever been observed before, and the frequency of such impacts (allowing for unobservability during solar conjunction) is less than one per 80 years." Using Asphaug and Benz's (1996) calculation that the SL9 parent was roughly 1.5–1.8 km, the largest fragments would have been on the order of 1 km across. So we take the historical record of direct hits as implying that there is a rough upper limit of <0.012 hits per annum with $d_c > 1 \pm 0.4$ km. This point is plotted on Figure 18.17 as "hits."

Centaurs

Another way to calibrate the JFCs is to link them to the Centaurs. There are three large Centaurs in Saturn-crossing orbits: Chiron, Pholus, and the lost 1995 SN55. All appear to be roughly 150–180 km diameter (Fernandez *et al.* 2002). Their annual Öpik impact probabilites with Saturn are 1.5×10^{-8}, 1.0×10^{-9}, and 3.5×10^{-9}, respectively. Added

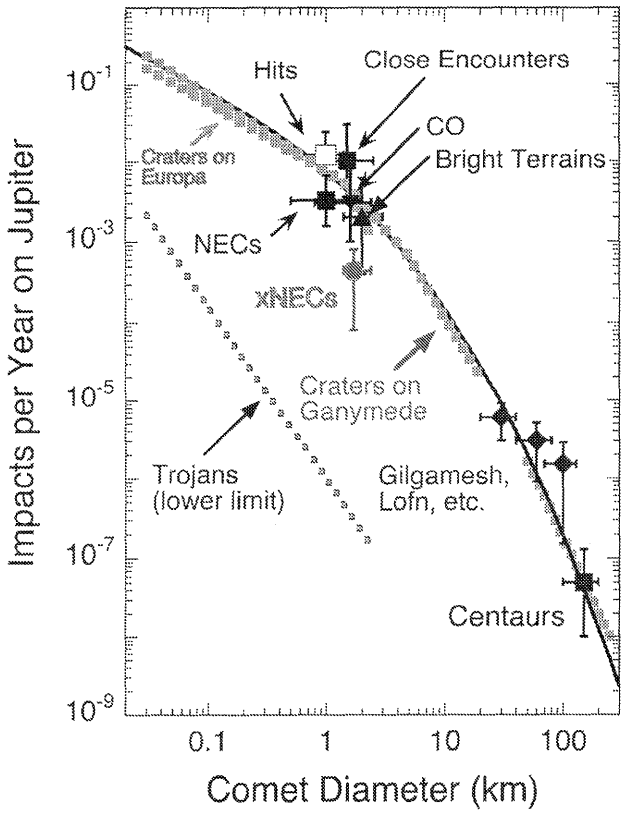

Figure 18.17. Cumulative impact rates at Jupiter. Impact rates on the Galilean satellites are ~10 000 times smaller. Points (with error bars) refer to impact rates at Jupiter, with the points labeled "Centaurs" scaled from the impact rate at Saturn. "Hits" refers to observed impacts (in 1994 and 1690); "Close Encounters" refers to the half-dozen comets known to have passed within 2 jovian radii of Jupiter's cloudtops; "CO" is the impact rate required to supply the observed excess of jovian stratospheric CO; "Bright Terrains" is the long-term average obtained using the number of 30 km craters on Ganymede's bright terrains (see text); "Gilgamesh, Lofn, etc." refers to the long-term average obtained using the four largest young basins on Ganymede and Callisto; "NECs" is the impact rate at Jupiter extrapolated from forty active Near-Earth Comets (Levison *et al.* 2000); and "xNECs" is the impact rate at Jupiter extrapolated from six extinct NECs (Bottke *et al.* 2002). The lines indicate size–frequency distributions obtained from small craters superposed on young surfaces on Europa and Ganymede (see Figure 18.16) and from the observed populations of Kuiper Belt Objects (plotted through the "Centaur" point). The "Trojans" line refers to the rate that Trojan asteroids would hit Jupiter if orbital dynamics were the only loss mechanism depleting the L4 and L5 swarms; it becomes a lower limit if collisions between rival Trojans are important. The solid black curve is the analytic approximation given in the text. Note that the size distribution deviates from a power law at Jupiter, such that both very large (>100 km) and small comets (<1 km) are relatively rare.

together they imply that 150-km objects hit Saturn 2×10^{-8} per annum. To scale this impact rate to Jupiter we use Levison *et al.*'s (2000) Saturn/Jupiter impact ratio of 0.4. This gives a corresponding impact rate of Chiron-scale comets on Jupiter of 5×10^{-8}. This point is plotted on Figure 18.17 as "Centaurs." To extend this to smaller sizes requires a size distribution. Here surveys of Kuiper Belt Objects are useful. Trujillo *et al.* (2001) determine a cumulative slope $b = 3 \pm 0.5$ for $d_c > 100$ km while Gladman *et al.* (2001) recommend a cumulative slope $b = 3.4 \pm 0.3$ for $d_c > 50$ km. Sheppard *et al.* (2000) argued that the same size distribution that holds for KBOs holds for Centaurs. Here we will take the average and use $b = 3.2$. We extend the slope to diameters as small as $d_c = 50$ km. This slope is plotted on Figure 18.17.

18.5.2 Crater Scaling

For crater scaling we use a simple expression that is based on apparent crater volumes obtained in the gravity-scaling regime by Schmidt and Housen (1987). For simple craters made by a comet of diameter d_c (in km) we use

$$D_t = 13.4 \left(\frac{v^2}{g}\right)^{0.217} \left(\frac{\rho_i}{\rho_t}\right)^{0.333} d_c^{0.783} \cos^{0.333}\theta \text{ km} \quad (18.4)$$

For complex craters we modify the above to take some account of the broader profile of the complex crater,

$$D = D_t^{\xi} D_c^{1-\xi} \quad (18.5)$$

where the diameter D_c ($D_c = 2.5$ km for Europa, Ganymede, and Callisto) refers to Transition I. The exponent $\xi \approx 1.13$ accounts for crater slumping. We evaluate these expressions using $\theta = 45°$ for the typical incidence angle. We assume an impactor density of $\rho_i = 0.6$ g cm^{-3}, consistent with the density of SL9 (Asphaug and Benz 1996), and a target density of $\rho_t = 0.9$ g cm^{-3}, consistent with ice. Typical impact parameters are given in Table 18.2.

18.5.3 Projectile Size Distributions

Zahnle *et al.* (2003) use crater populations on Europa, Gilgamesh, and Lofn reported here (see Figure 18.16) to obtain the size–number distribution of small comets at Jupiter. Based on ~100 craters with $D > 1$ km, Zahnle *et al.* (2003) infer a cumulative comet size distribution $N(> d_c) \propto d_c^{-b}$ with $b = 0.9$ for $d_c < 1$ km. The distribution may steepen significantly for $d_c > 1$ km (craters bigger than 20 km), but there are few craters in this range in the data set (~11% of the surface). This slope is plotted on Figure 18.17 as "Europa."

Crater densities on Gilgamesh and Lofn are higher than on Europa. Larger secondaries are unlikely to be a problem, however, due to the lack of large impact features postdating these structures. From craters on the Gilgamesh ejecta blanket, the inferred slope of the power-law distribution is $1 < b < 1.2$ for $d_c < 2$ km. A similar distribution applies to Lofn. Overall we see a consistent picture of a production population that is greatly depleted of small objects compared to most other solar system populations.

Larger craters tell a different story. From the global count of craters on Ganymede with $D > 30$ km, about half are found on the bright terrains. Because the crater density is lower on the bright terrains than it is on the older dark terrains or on Callisto, we will begin by assuming that the observed crater diameter distribution approximates the production population. If we do this we infer that for comet sizes $2 < d_c < 5$ km the effective slope is $b = 1.7$, and for $5 < d_c < 20$ km the slope is $b \approx 2.5$. Above this size there

Table 18.2. Impact parameters for the jovian satellites.

Moon	Imp. vel. [km s^{-1}]	Target Density	D_c* [km]	gravity [cm s^{-2}]	Rel. Imp. Rate [*vs.* Jupiter]	Disruption Time [Gyr]
Metis	59	1.0	15	1.4	2.8E−07	0.8
Amalthea	50	1.0	15	2.6	7.7E−07	1.6
Thebe	45	1.0	15	0.6	2.9E−08	2.4
Io	32.3	2.7	15	181	1.4E−04	
Europa	25.5	0.9	2.5	130	6.6E−05	
Ganymede	20.4	0.9	2.5	143	1.2E−04	
Callisto	15.4	0.9	2.5	125	6.1E−05	
Himalia	6.1	1.5	15	3.8	1.4E−08	

* Transition diameters for small satellites assumed similar to those of mid-sized saturnian satellites (Schenk 1989).

are but two craters. This slope is plotted on Figure 18.17 as "Craters on Ganymede."

It seems that the size distribution of comets changes dramatically between $1 < d_c < 2$ km, but there are too few data to define at exactly what size the change occurs (Zahnle *et al.* 2003). The change in slope at $d_c \approx 5$ km (corresponding to 60 km diameter craters) may be an artifact of saturation. The slope of the size distribution of KBOs with $d_c > 50$ km is apparently even steeper, $b \approx 3.2$ (Trujillo *et al.* 2001, Gladman *et al.* 2001). A zeroth-order reading of the data shows a monotonic increase in the slope as d_c increases, from $b \approx 1$ for $d_c < 1$ km, rising to $b \approx 3.2$ for $d_c > 50$ km, and passing through $b \approx 1.7$ for $2 < d_c < 5$ and $b \approx 2.5$ for $5 < d_c < 20$. A good approximation to the cumulative size distribution for $0.03 < d_c < 300$ km and the collision rate per annum with Jupiter is

$$N(>d_c) = 0.004\,(d_c/1.5\text{ km})^{-b(d_c)} \tag{18.6}$$

where

$$b(d_c) = 0.9 + 0.32\ln(d_c/1\text{ km}) + 0.015\,[\ln(d_c/200\text{ km})]^2 \tag{18.7}$$

Figure 18.17 compares this fit to the deduced size distribution. This fit should not be applied to comets bigger than 300 km nor smaller than 30 m. The calibration to the inferred impact rate at Jupiter is conservative, and probably uncertain by at least a factor of three.

18.5.4 Absolute Cratering Rates

From the Craters Themselves

The most direct estimate of cratering rates in the jovian system is based on the craters themselves and presumptions about the onset of secular cooling in Ganymede. The simplest and most conservative estimate is to presume that the bright terrains are less than 4 Gyr (e.g., Neukum *et al.* 1999). The observed average density of 30 km impact craters on bright terrains on Ganymede is $N(>30\text{ km}) = 10$ per 10^6 km^2. The typical 30 km crater on Ganymede is made by a $d_c = 2.4 \pm 0.5$ km diameter comet. Using 1.2×10^{-4} as the ratio of global impact rates on Ganymede to Jupiter (Table 18.2), the average rate that $d_c \geq 2.0$ km comets struck Jupiter over the past 4 Gyr is 2×10^{-3} per year. This is obviously a lower limit. It is plotted on Figure 18.17 labeled by "Bright Terrains".

We can make a similar argument for the largest young basins on Ganymede and Callisto. Gilgamesh has a diameter of ~590 km, implying a ~60 km diameter comet. The next largest young basin on Ganymede, with a diameter ~350 km, is found near the south pole ($\beta = 98°$) on bright terrain and has been nameless. It requires a ~30 km comet. Callisto also has two large young basins. Valhalla, at ~1000 km, is the product of a ~100 km comet. Valhalla is more heavily cratered than Lofn or Gilgamesh, but it is also near the apex of motion, where cratering rates are especially high. Lofn (Chapter 17), with a diameter of ~355 km (Section 18.2.1), can be attributed to a ~35 km comet. Asgard, estimated at ~680 km diameter, can be attributed to a ~70 km comet, but is significantly older than Valhalla (e.g., Wagner *et al.* 1999).

Thus on Ganymede and Callisto there are only 4 young impacts with $d_c > 30$ km. Together, Ganymede and Callisto are struck 1.8×10^{-4} as often as Jupiter. Spread over 4 Gyr these 4 comets imply an impact rate on Jupiter of $\dot{N}(d_c > 30 \pm 10\text{ km}) = 6 \pm 3 \times 10^{-6}$ per annum. Similar rates can be deduced for the two comets with $d_c > 60$ km and the 1 comet with $d_c \sim 100$ km. These rates are plotted on Figure 18.17.

18.5.5 Asteroids

Shoemaker *et al.* (1989) estimated that there are ~2000 Trojan asteroids with $d_c > 17$ km (albedo of 0.04). According to Shoemaker *et al.* (1989) Trojans smaller than 100 km follow a $b = 2.17$ power law and the larger ones follow a much steeper $b = 3.75$ power law. Shoemaker *et al.*'s estimate is equivalent to 390 000 Trojans with $d_c > 1.5$ km. More recently Jewitt *et al.* (2000) estimate that there are 160 000 Trojans librating around L4 with diameters $d_c > 2$ km, with $b = 2 \pm 0.3$. This estimate extrapolates to 570 000 Trojans with $d_c > 1.5$ km (assuming the L4 and L5 swarms are equal).

Levison *et al.* (1997) found that the dynamical lifetime of the average Trojan asteroid is 35 billion years. Levison and Duncan (1997) showed that 2% of JFC-like test particles hit Jupiter. If we presume that the same fraction applies to escaped Trojans, and combine this with Jewitt *et al.*'s (2000) numbers and Shoemaker *et al.*'s (1989) size distributions, we obtain an annual impact rate of 1.5 km Trojans on Jupiter of 4×10^7 per annum. This is about four orders of magnitude smaller than the corresponding JFC impact rate. These are plotted on Figure 18.17 as a lower limit.

To raise this rate appreciably requires that Trojans be mostly ejected by collisions. Collisional ejection has been

proposed (Marzari *et al.* 1998). Small bodies are more likely to be collisionally ejected. This makes the obviously non-collisional shallow slope of craters much bigger than 1 km on Europa an argument against the Trojans currently being important at these sizes. Trojans would be important at the 100 m scale if collisional ejection reduces the Trojan lifetime at least a hundred-fold, to less than 350 Myr. Such a short lifetime would likely make Trojans important at all scales everywhere > 3.5 Gyr.

18.5.6 Summary of Surface Ages

In this section we summarize published and proposed crater retention ages for the jovian satellites and selected features. Cratering rates are from Zahnle *et al.* (2003). For 10 km craters the new rates are typically about 70% of those recommended by Shoemaker, but for 30 km craters the new rates are about twice as great as Shoemaker's. These differences are mostly attributable to different size–number distributions of comets. Alternative dates are from Neukum *et al.* (1999) and Wagner *et al.* (1999).

Small Satellites

Metis, Thebe, and Amalthea all have timescales against collisional disruption that are measured in the billions of years and it is unlikely that all three have survived 4 Gyr unscathed in their present form in their present orbits (Table 18.2, see Zahnle *et al.* 2003).

Io

Voyager medium-resolution and *Galileo* medium- and high-resolution observations have thus far failed to reveal any impact craters on the surface. Indeed, not even partially buried crater-like forms have been reported. If we take regional scale images covering ~15% of the surface and averaging 250–400 m/pixel as our mapping base, the smallest craters that could be reliably mapped would be on the order of 5 km. If we extrapolate this null result over the entire surface, Zahnle *et al.*'s (2003) model age for Io would be 0.3 Myr. In crater removal, what matters is rim height above ground level; once a crater wall is breached the depression may be easily filled in to ground level. Given that impact craters on silicate-rich Io would probably resemble lunar craters, complete burial of all 5 km craters (rim heights of ~200 m, Pike 1980) would require a minimum globally integrated resurfacing rate of ~0.07 cm yr^{-1}.

A more conservative estimate based on a best average global resolution of 2 km suggests that there are no craters 20 km or larger (Chapter 14). The corresponding model age is 2.3 Myr. Burial of all 20-km craters (rim height ~700 m, Pike 1980) over 2.3 Myr would require a minimum global resurfacing rate of ~0.03 cm yr^{-1}.

Europa

Neukum *et al.* (1999) model ages for Europa range from 1 to 3 Ga. Ages for chaos regions may be half that (Neukum *et al.* 1998), but Conamara Chaos is peppered with Pwyll secondaries and age dating seems problematical at best. Zahnle *et al.*'s (2003) model ages for Europa are significantly older than the 10 Ma estimated by Zahnle *et al.* (1998). The average crater density is ~30 ($D > 1$ km) per 10^6 km^2, and the corresponding nominal surface age is 60 Ma. An alternative approach is to use large craters. The best current estimate for the global number of 20-km craters on Europa is about 10, but again the imaging coverage is incomplete and highly variable in resolution. If we extrapolate the number (3) of 20 km craters in the uniform resolution counting area to the entire surface area, we can estimate there are as many as 27 such craters on Europa. At an average rate of one 20 km crater per 2.3 Ma (Zahnle *et al.* 2003), we would pick an average age of Europa's surface c. 60 Ma. Shoemaker and Wolfe's (1982) cratering rates are higher than Zahnle *et al.* (2003) for small craters because the former assumed that a single master power law of form $N(> d_c) \propto d_c^{-2}$ extended to indefinitely small sizes. This proved a poor assumption, as Ivanov *et al.* (1998) pointed out. Comets small enough to make 10-km craters are rarer in our distribution.

Obvious secondaries were discarded from our count of km-size craters on Europa. Planetocentric cratering caused by ejecta launched into jovicentric orbit cannot be completely excluded; these craters would not cluster or line up along crater rays as secondaries do. Such planetocentric secondaries would be indistinguishable from primary craters. If present, they would imply an even younger surface for Europa. However, classical secondary craters are known to have a steep size–frequency distribution akin to a collisional population (e.g., Melosh 1989), and presumably the same is true of planetocentric debris (e.g., Croft *et al.* 1995). The shallow slope of the 1–10 km diameter europan craters would seem to exclude significant numbers of secondaries of either type in that size range. Moreover, the largest ordinary secondaries are typically only about 4% the diameter of the primary crater (Melosh 1989, p. 101); on Europa the largest secondaries are likely to be 2 km across. In a discussion of the ganymedean Gilgamesh impact, by scaling from large lunar and vestal craters, Alvarellos *et al.* (2002) estimated that the largest blocks launched at escape velocity would have been on the order of 1 km, typically making 4 km craters on Ganymede. Scaling by the size of the primary craters implies that we should not expect planetocentric secondaries to be important on Europa at sizes larger than about 500 meters.

Ganymede

Because resurfacing on Ganymede may (or may not) be tied to orbital evolution, a determination of surface ages is of great interest to geologists and Jupiter system dynamicists alike (Chapters 13 and 16). Neukum *et al.* (1998) assign ages of 3.6 to 4.2 Gyr for bright and dark terrains respectively. Zahnle *et al.* (2003) revise their ages for younger bright terrain to ~2 Gyr based on the average crater density reported here. It will then have been ~1 Gyr since nonsynchronous rotation stopped. These ages are very uncertain.

The age of Gilgamesh is perhaps more interesting. Neukum *et al.* (1998) and Wagner *et al.* (1999) assume an age of 3.8 Gyr for Gilgamesh but also dismiss the younger ages reported for Gilgamesh and similar large impact features by Zahnle and others, based on their own assumption that these impact features formed very early. Crater densities on the ejecta blanket, although lower than bright terrains, are much higher than the crater densities on Europa.

Assume that Gilgamesh post-dates synchronicity (rather than coincides with LHB), as could be the case given that Gilgamesh postdates bright terrain which nonsynchronicity is provisionally tied to by orbital dynamics (e.g., Showman and Malhotra 1997). The local cratering rate at $\beta = 65°$ is about 45% higher than the global average. The age that results is 700 Ma (Zahnle *et al.* 2003). If Gilgamesh predates nonsychronicity, as seems likely, this age increases by as much as 45%.

Callisto

Callisto's cratered surfaces are by all measures ancient (with subtle variations in absolute ages that are of little critical importance). Neukum *et al.* (1998) and Wagner *et al.* (1999) report an age of 4 to 4.3 Gyr for various regions of Callisto, and ages of 3.9 to 4.2 Gyr for impact features such as Lofn, Valhalla, and Asgard (Wagner *et al.* 1999). Zahnle *et al.* agree that the surface of Callisto is ancient. However, the multi-ring features Lofn and Valhalla appear to be much younger in Zahnle's chronology. Both Lofn and Valhalla are assigned nominal ages of ~2 Gyr (Zahnle *et al.* 2003), although the young age is very uncertain for Valhalla, which is more densely cratered. Because Valhalla is near the apex of motion cratering rates are high so that dense cratering does not in itself imply deep age. The young age treats the density of small craters as a production population, which is an iffy proposition.

18.5.7 Just How Old Are Galilean Satellite Surfaces?

The basic choice between the Shoemaker–Zahnle view and the Neukum view of the cratering records is whether to look backward from the observable present or forward from an assumed past. As presented here the Shoemaker–Zahnle model assumes a constant cometary flux back a few billion years. Even younger ages would result if the comet flux has decayed with time, or if other cratering populations were much more important in the past than they are now. The masses of comets remain an uncertainty but one that future comet missions can address. There remains considerable uncertainty in how far back in time the current flux can be extrapolated. A young (~60 Myr) age for Europa is probably safe (within a factor of 3) as it is unlikely that the present dynamical conditions, dominated by ecliptic comets, have changed very much over the past 10 Myr or so. This places Europa's average surface in the most recent few percent of solar system history. The much older ages of 1–3 Ga favored by Neukum are wholly inconsistent with the known numbers and dynamics of small solar system bodies and would push us away from a geologically active Europa. The young ages for bright terrain on Ganymede are more uncertain yet fundamental to jovian satellite history.

The Neukum model, which assumes asteroidal populations and fluxes and LHB timing, suffers from what we view as fundamental difficulties, principally the lack of observational constraints and the somewhat arbitrary imposition of specific ages to features such as Gilgamesh. The arguable *Voyager*-era similarity of size–frequency distributions between the inner and outer solar system (cf. Chapman and McKinnon 1986, Ivanov *et al.* 2002) is now less similar (Figure 18.14) because of the under-representation of large impact features and depletion of small craters. Even if they were similar, they would not necessarily imply the same source population. As noted, the current flux is demonstrably cometary. The earliest flux, on which the Neukum view rests, could have been dominated by asteroids, but this has not been demonstrated for the jovian satellites (moreover, if it was asteroidal, our ages based on comets alone become underestimates). Neukum *et al.* (1999) also argue that the abundance of small (<1 km) craters is contrary to the apparent observational lack of tiny (<100 m) comets. The evidence that most small craters on Europa are secondaries (Bierhaus *et al.* 2001) makes this argument irrelevant. In our opinion the only real reason for proposing that Gilgamesh and other multi-ring features were formed by asteroids at the same time as the large lunar basins is that they are themselves large impact features. Our estimates of the projectile diameter (~60 ± 20 km across) for Gilgamesh make P/Hale–Bopp (Weaver and Lamy 1999) comparable to, but smaller than the larger Centaurs. Only 4 such Hale–Bopp class impacts have been identified on Ganymede and Callisto (see above). Obviously such large cometary projectiles are available, and an asteroidal source is not required.

18.6 TO BE LEARNED

Our view of the history of the Galilean satellites (and the solar system for that matter) is not likely to survive the shelf life of this volume completely intact. First among the offenders is observational data and the completeness of the solar system inventory. Obviously a better understanding of the numbers, sizes and masses of JFCs is needed, and this can only be accomplished with the passage of time, especially telescope time. On the satellites themselves, image coverage is limited and flawed. Are the few high-resolution areas sampled representative or are some contaminated by secondaries from nearby unseen craters or differential degradation processes? Are there trends with latitude or longitude that have gone unobserved? Differences in the size–frequency distribution on the leading and trailing hemispheres may ultimately help determine whether two different populations were involved in cratering Ganymede. Better imaging at Ganymede's antapex, uncorrupted by image compression artifacts, is required here.

An important result from crater morphology is that morphology and shape can be used to probe the lithospheres of these bodies. A confirmation of the europan ocean as suggested by the transition to multi-ring craters is top of the list of targets. But the global survey (~11% complete) of impact craters on Europa is far from satisfactory. How many large craters are there, what are their sizes and morphologies, and how are they distributed? Are there any craters with morphologies transitional between complex craters (Pwyll) and multi-ring features (Callanish)? Is there any indication that these transitions might have changed over time on Europa? Some larger craters were observed on Europa but could not be characterized. In short, a second Jupiter orbiter capable of completing *Galileo*'s original global mapping mission at resolutions of 100 m/pixel or better should be a top priority.

Ideally, we desire some sort of independent calibration for the impact cratering timescales. Zahnle *et al.* (2003)

explore some potential calibration methods reviewed here, but each is fraught with uncertainty. A datable sample from one of the Galilean satellites could anchor the age models for all the other satellites. Contrary to expectation, we might argue for a sample of Ganymede's bright terrain, rather than attempt to extrapolate an age from Europa's very young surface to the ancient surfaces of Ganymede and Callisto.

The Galilean satellite cratering record also allows us the indiscretion of anticipating *Cassini* discoveries at Titan and the other Saturnian satellites. Titan's atmosphere limits crater sizes but small craters would obviously indicate a thinner atmosphere in the past. Interference of the atmosphere with ejecta could produce unusual surface patterns similar to those observed on Venus. Pedestal or other "flow-like" morphologies similar to those on Ganymede should occur on Titan but might not occur on the smaller satellites if pedestals are related to creep or flow of warm ice, with or without impact melt. Titan is so similar in size to Ganymede and Callisto that we would expect the depth/diameter curve (if measurable) to resemble that of these two icy satellites. Morphology should follow suit. Original crater depths and rim heights will be shallow (<1.5 and <1.0 km, respectively) and observed depths and rim heights could be used for estimating the thickness of sediment fill, relaxation, lake depths, etc. (e.g., Lorenz 1994). Obviously, the size–frequency distribution of craters on Titan will be of interest to compare with the jovian system. Does the large crater population in the Saturn system resemble that of the Jupiter system or does the Saturn system record two separate populations as some have proposed (e.g., Smith *et al.* 1981)? We eagerly anticipate cratering results from the entire Saturn family, as well as the return to Jupiter to complete the missions of the two *Galileo*s.

Acknowledgements. We thank B. Bierhaus, W. Merline, P. Weissman, L. Dones, and H. Levison for their fundamental contributions, Boris Ivanov and an anonymous reviewer for their comments. Some of the work reported here was supported by the *Galileo* SSI Team and by the NASA jovian System Data Analysis and Planetary Geology and Geophysics Programs.

REFERENCES

Alvarellos, J. L., K. J. Zahnle, A. R. Dobrovolskis, and P. Hamill, Orbital evolution of impact ejecta from Ganymede, *Icarus* **160**, 108–123, 2002.

Anderson, J. D., R. A. Jacobson, T. P. McElrath, W. B. Moore, G. Schubert, and P. C. Thomas, Shape, mean radius, gravity field, and interior structure of Callisto, *Icarus* **153**, 157–161, 2001.

Asphaug, E. and W. Benz, Size, density, and structure of Comet Shoemaker–Levy 9 inferred from the physics of tidal breakup, *Icarus* **121**, 225–248, 1996.

Barlow, N. G., J. M. Boyce, F. M. Costard, R. A. Craddock, J. B. Garvin, S. E. H. Sakimoto, R. O. Kuzmin, D. J. Roddy, and L. A. Soderblom, Standardizing the nomenclature of martian impact crater ejecta morphologies, *J. Geophys. Res.* **105**, 26 733–26 738, 2000.

Bezard, B., E. Lellouch, D. Strobel, J. Maillard, and P. Drossart, Carbon monoxide on Jupiter: Evidence for both internal and external sources, *Icarus* **159**, 95–111, 2002.

Bierhaus, E. B., C. R. Chapman, W. J. Merline, R. Greeley, and J. Klemaszewski, Small crater populations on Callisto, in *Lunar and Planetary Science Conference Abstracts*, p. 1996, 2000.

Bierhaus, E. B., C. R. Chapman, W. J. Merline, S. M. Brooks, and E. Asphaug, Pwyll secondaries and other small craters on Europa, *Icarus* **153**, 264–276, 2001.

Bottke, W. F., A. Morbidelli, R. Jedicke, J. Petit, H. F. Levison, P. Michel, and T. S. Metcalfe, Debiased orbital and absolute magnitude distribution of the near-Earth objects, *Icarus* **156**, 399–433, 2002.

Chapman, C. R. and W. B. McKinnon, Cratering of planetary satellites, in *Satellites*, J. A. Burns, M. S. Matthews (eds), University of Arizona Press, pp. 492–580, 1986.

Chapman, C. R., W. J. Merline, B. Bierhaus, S. Brooks, and *Galileo* Imaging Team, Cratering in the jovian system: Intersatellite comparisons, in *Lunar and Planetary Science Conference Abstracts*, p. 1927, 1998.

Croft, S. K., A proposed origin for palimpsests and anomalous pit craters on Ganymede and Callisto, *J. Geophys. Res.* **88**, 71–89, 1983.

Croft, S. K., J. Kargel, R. Kirk, J. Moore, P. Schenk, and R. Strom, The geology of Triton, in *Neptune and Triton*, D. P. Cruikshank (ed), University of Arizona Press, pp. 879–947, 1995.

DeHon, R. A., A. C. Leith, and W. B. McKinnon, Geologic map of the Hathor Region (Jg-15) of Ganymede, *U.S.G.S. Misc. Invest. Series* **I-2388**, 1994.

Dombard, A. J. and W. B. McKinnon, Long-term retention of impact crater topography on Ganymede, *Geophys. Res. Lett.* **27**, 3663–3666, 2000.

Duncan, M. J. and H. F. Levison, A scattered comet disk and the origin of Jupiter family comets, *Science* **276**, 1670–1672, 1997.

Durham, W. B. and L. A. Stern, Rheological properties of water ice: Applications to satellites of the outer planets, *Ann. Rev. Earth Planet. Sci.* **29**, 295–330, 2001.

Fernández, Y. R., D. C. Jewitt, and S. S. Sheppard, Thermal properties of centaurs Asbolus and Chiron, *AJ* **123**, 1050–1055, 2002.

Gault, D. E. and J. A. Wedekind, Experimental studies of oblique impact, in *Lunar and Planetary Science Conference*, pp. 3843–3875, 1978.

Geissler, P. E., R. Greenberg, G. Hoppa, P. Helfenstein, A. McEwen, R. Pappalardo, R. Tufts, M. Ockert-Bell, R. Sullivan, and R. Greeley, Evidence for non-synchronous rotation of Europa, *Nature* **391**, 368, 1998.

Gladman, B., J. J. Kavelaars, J. Petit, A. Morbidelli, M. J. Holman, and T. Loredo, The structure of the Kuiper Belt: Size distribution and radial extent, *AJ* **122**, 1051–1066, 2001.

Greeley, R., J. H. Fink, D. E. Gault, and J. E. Guest, Experimental simulation of impact cratering on icy satellites, in *Satellites of Jupiter*, D. Morrison (ed), University of Arizona Press, pp. 340–378, 1982.

Greeley, R., S. Heiner, and J. E. Klemaszewski, Geology of Lofn Crater, Callisto, *J. Geophys. Res.* **106**, 3261–3274, 2001.

Greenberg, R. and S. J. Weidenschilling, How fast do Galilean satellites spin?, *Icarus* **58**, 186–196, 1984.

Hartmann, W., Planetary cratering: I. Lunar highlands and tests of hypotheses on crater populations, *Meteoritics* **30**, 451, 1995.

Hartmann, W. K., Does crater 'saturation equilibrium' occur in the solar system?, *Icarus* **60**, 56–74, 1984.

Hawke, B. R. and J. F. Bell, Remote sensing studies of lunar dark-halo craters, *BAAS* **13**, 712, 1981.

Hillgren, V. J. and H. J. Melosh, Crater relaxation on Ganymede: Implications for ice rheology, *Geophys. Res. Lett.* **16**, 1339–1342, 1989.

Horedt, G. P. and G. Neukum, Cratering rate over the surface of a synchronous satellite, *Icarus* **60**, 710–717, 1984.

Horner, V. M. and R. Greeley, Pedestal craters on Ganymede, *Icarus* **51**, 549–562, 1982.

Ivanov, B. A., G. Neukum, and D. Deniem, Cometary impact rates on jovian satellites: Questions, in *Lunar and Planetary Science Conference Abstracts*, p. 1769, 1998.

Ivanov, B. A., G. Neukum, W. F. Bottke, and W. K. Hartmann, The comparison of size–frequency distributions of impact craters and asteroids and the planetary cratering rate, in *Asteroids III*, W. F. Bottke Jr., A. Cellino, P. Paolicchi, and R. P. Binzel (eds), University of Arizona Press, Tucson, pp. 89–101, 2002.

Jewitt, D. C., C. A. Trujillo, and J. X. Luu, Population and size distribution of small jovian Trojan asteroids, *AJ* **120**, 1140–1147, 2000.

Johnson, T. V. and T. R. McGetchin, Topography on satellite surfaces and the shape of asteroids, *Icarus* **18**, 612–620, 1973.

Jones, K. B., J. W. Head, R. T. Pappalardo, and J. M. Moore, Morphology and origin of palimpsests on Ganymede from Galileo observations, *Icarus* **164**, 188–198, 2003.

Kivelson, M. G., K. K. Khurana, and M. Volwerk, The permanent and inductive magnetic moments of Ganymede, *Icarus* **157**, 507–522, 2002.

Kronk, G. W., *Comets: A Descriptive Catalog*, Enslow, 1984.

Lellouch, E., B. Bézard, R. Moreno, D. Bockelée-Morvan, P. Colom, J. Crovisier, M. Festou, D. Gautier, A. Marten, and G. Paubert, Carbon monoxide in Jupiter after the impact of Comet Shoemaker–Levy 9, *Planet. Space Sci.* **45**, 1203–1212, 1997.

Levison, H. F., Comet taxonomy, in *Completing the Inventory of the Solar System*, T. W. Rettig, J. M. Hahn (eds), pp. 173–191, ASP Conf. 107, 1996.

Levison, H. F. and M. J. Duncan, From the Kuiper Belt to Jupiter-Family Comets: The spatial distribution of ecliptic comets, *Icarus* **127**, 13–32, 1997.

Levison, H. F., M. J. Duncan, K. Zahnle, M. Holman, and L. Dones, Planetary impact rates from ecliptic comets, *Icarus* **143**, 415–420, 2000.

Lorenz, R. D., Crater lakes on Titan: Rings, horseshoes and bullseyes, *Planet. Space Sci.* **42**, 1–4, 1994.

Malhotra, R., Tidal origin of the Laplace resonance and the resurfacing of Ganymede, *Icarus* **94**, 399–412, 1991.

Marzari, F., E. Dotto, D. R. Davis, S. J. Weidenschilling, and V. Vanzani, Modelling the disruption and reaccumulation of Miranda, *A&A* **333**, 1082–1091, 1998.

McEwen, A. S., Tidal reorientation and the fracturing of Jupiter's moon Europa, *Nature* **321**, 49–51, 1986.

McKenzie, D., P. G. Ford, F. Liu, and G. H. Pettengill, Pancake-like domes on Venus, *J. Geophys. Res.* **97**, 15,967, 1992.

McKinnon, W. B., Mystery of Callisto: Is it undifferentiated?, *Icarus* **130**, 540–543, 1997.

McKinnon, W. B. and H. J. Melosh, Evolution of planetary lithospheres: Evidence from multiringed structures on Ganymede and Callisto, *Icarus* **44**, 454–471, 1980.

McKinnon, W. B. and P. M. Schenk, Estimates of comet fragment masses from impact crater chains on Callisto and Ganymede, *Geophys. Res. Lett.* **22**, 1829–1832, 1995.

McKinnon, W. B., C. R. Chapman, and K. R. Housen, Cratering of the Uranian satellites, in *Uranus*, J. T. Berstalh, E. D. Miner and M. S. Matthews (eds), University of Arizona Press, pp. 629–692, 1991.

Melosh, H. J., *Impact Cratering: A Geologic Process*, Oxford University Press, 1989.

Melosh, H. J. and B. A. Ivanov, Impact crater collapse, *Ann. Rev. Earth Planet. Sci.* **27**, 385–415, 1999.

Melosh, H. J. and P. Schenk, Split comets and the origin of crater chains on Ganymede and Callisto, *Nature* **365**, 731, 1993.

Moore, J. M. and M. C. Malin, Dome craters on Ganymede, *Geophys. Res. Lett.* **15**, 225–228, 1988.

Moore, J. M., E. Asphaug, R. J. Sullivan, J. E. Klemaszewski, K. C. Bender, R. Greeley, P. E. Geissler, A. S. McEwen, E. P. Turtle, C. B. Phillips, B. R. Tufts, J. W. Head, R. T. Pappalardo, K. B. Jones, C. R. Chapman, M. J. S. Belton, R. L. Kirk, and D. Morrison, Large impact features on Europa: Results of the *Galileo* Nominal Mission, *Icarus* **135**, 127–145, 1998.

Moore, J. M., E. Asphaug, D. Morrison, J. R. Spencer, C. R. Chapman, B. Bierhaus, R. J. Sullivan, F. C. Chuang, J. E. Klemaszewski, R. Greeley, K. C. Bender, P. E. Geissler, P. Helfenstein, and C. B. Pilcher, Mass movement and landform degradation on the icy Galilean satellites: Results of the *Galileo* Nominal Mission, *Icarus* **140**, 294–312, 1999.

Moore, J. M., E. Asphaug, M. J. S. Belton, B. Bierhaus, H. H. Breneman, S. M. Brooks, C. R. Chapman, F. C. Chuang, G. C. Collins, B. Giese, R. Greeley, J. W. Head, S. Kadel, K. P. Klaasen, J. E. Klemaszewski, K. P. Magee, J. Moreau, D. Morrison, G. Neukum, R. T. Pappalardo, C. B. Phillips, P. M. Schenk, D. A. Senske, R. J. Sullivan, E. P. Turtle, and K. K. Williams, Impact features on Europa: Results of the *Galileo* Europa Mission (GEM), *Icarus* **151**, 93–111, 2001.

Murchie, S. L., J. W. Head, and J. B. Plescia, Crater densities and crater ages of different terrain types on Ganymede, *Icarus* **81**, 271–297, 1989.

Neukum, G., Cratering records of the satellites of Jupiter and Saturn, *Adv. Space Res.* **5**, 107–116, 1985.

Neukum, G., R. Wagner, U. Wolf, B. A. Ivanov, J. W. Head, R. T. Pappalardo, J. E. Klemaszewski, R. Greeley, M. J. S. Belton, and *Galileo* SSI Team, Cratering chronology in the jovian system and derivation of absolute ages, in *Lunar and Planetary Science Conference Abstracts*, p. 1742, 1998.

Neukum, G., R. Wagner, U. Wolf, and the *Galileo* SSI Team, Cratering record of Europa and implications for timescale and crustal development, in *Lunar and Planetary Science Conference Abstracts*, p. 1992, 1999.

Passey, Q. R. and E. M. Shoemaker, Craters and basins on Ganymede and Callisto: Morphological indicators of crustal evolution, in *Satellites of Jupiter*, D. Morrison (ed), University of Arizona Press, pp. 379–434, 1982.

Pike, R. J., Size-dependence in the shape of fresh impact craters on the Moon, in *Impact and Explosion Cratering*, D. J. Roddy, R. O. Pepin, R. B. Merrill (eds), Pergamon Press, pp. 489–509, 1977.

Pike, R. J., Control of crater morphology by gravity and target type: Mars, Earth, Moon, in *Lunar and Planetary Science Conference*, pp. 2159–2189, 1980.

Pike, R. J., Geomorphology of impact craters on Mercury, in *Mercury*, F. Vilas, C. R. Chapman, M. S. Matthews (eds), University of Arizona Press, pp. 165–273, 1988.

Prockter, L. M., J. W. Head, R. T. Pappalardo, D. A. Senske, G. Neukum, R. Wagner, U. Wolf, J. O. Oberst, B. Giese, J. M. Moore, C. R. Chapman, P. Helfenstein, R. Greeley, H. H. Breneman, and M. J. S. Belton, Dark terrain on Ganymede: Geological mapping and interpretation of *Galileo* Regio at high resolution, *Icarus* **135**, 317–344, 1998a.

Prockter, L. M., D. Senske, J. W. Head, R. T. Pappalardo, G. C. Collins, R. Greeley, and *Galileo* SSI Team, Furrow systems on Ganymede: Morphology, evolution and distribution, in *Lunar and Planetary Science Conference Abstracts*, p. 1862, 1998b.

Rogers, J. H., The comet collision with Jupiter: II. The visible scars, *J. British Astron. Assoc.* **106**, 125–149, 1996.

Schenk, P., Origins of palimpsests and impact basins on Ganymede, in *Lunar and Planetary Science Conference Abstracts*, p. 1137, 1996.

Schenk, P. and S. Sobieszczyk, Cratering asymmetries on Ganymede and Triton: From the sublime to the ridiculous, *BAAS* **31**, 1182, 1999.

Schenk, P., W. McKinnon, and J. Moore, Stereo topography of Valhalla and Gilgamesh, in *Lunar and Planetary Institute Conference Abstracts*, p. 1249, 1997.

Schenk, P. M., Crater formation and modification on the icy satellites of Uranus and Saturn: Depth/diameter and central peak occurrence, *J. Geophys. Res.* **94**, 3813–3832, 1989.

Schenk, P. M., Ganymede and Callisto: Complex crater formation and planetary crusts, *J. Geophys. Res.* **96**, 15 635, 1991.

Schenk, P. M., Central pit and dome craters: Exposing the interiors of Ganymede and Callisto, *J. Geophys. Res.* **98**, 7475–7498, 1993.

Schenk, P. M., The geology of Callisto, *J. Geophys. Res.* **100**, 19 023–19 040, 1995.

Schenk, P. M., Thickness constraints on the icy shells of the Galilean satellites from a comparison of crater shapes, *Nature* **417**, 419–421, 2002.

Schenk, P. M. and W. B. McKinnon, Dark halo craters and the thickness of grooved terrain on Ganymede, *J. Geophys. Res.* **90**, 775–783, 1985.

Schenk, P. M. and J. M. Moore, Geologic landforms and processes on icy satellites, in *Solar System Ices*, B. Schmitt, C. de Bergh, M. Festou (eds), Kluwer, p. 551, 1998.

Schenk, P. M. and F. J. Ridolfi, Morphology and scaling of ejecta deposits on icy satellites, *Geophys. Res. Lett.* **29**, 31–1, 2002.

Schenk, P. M., E. Asphaug, W. B. McKinnon, H. J. Melosh, and P. R. Weissman, Cometary nuclei and tidal disruption: The geologic record of crater chains on Callisto and Ganymede, *Icarus* **121**, 249–274, 1996.

Schmidt, R. M. and K. R. Housen, Some recent advances in the scaling of impact and explosion cratering, *Int. J. Impact Eng.* **5**, 543–560, 1987.

Sheppard, S. S., D. C. Jewitt, C. A. Trujillo, M. J. I. Brown, and M. C. B. Ashley, A wide-field CCD survey for Centaurs and Kuiper Belt objects, *AJ* **120**, 2687–2694, 2000.

Shoemaker, E. M. and R. F. Wolfe, Cratering time scales for the Galilean satellites, in *Satellites of Jupiter*, D. Morrison (ed), University of Arizona Press, pp. 277–339, 1982.

Shoemaker, E. M., B. K. Lucchitta, D. E. Wilhelms, J. B. Plescia, and S. W. Squyres, The geology of Ganymede, in *Satellites of Jupiter*, D. Morrison (ed), University of Arizona Press, pp. 435–520, 1982.

Shoemaker, E. M., C. S. Shoemaker, and R. F. Wolfe, Trojan asteroids: Populations, dynamical structure and origin of the L4 and L5 swarms, in *Asteroids II*, R. P. Binzel, T. Gehrels, M. S. Matthews (eds), University of Arizona Press, pp. 487–523, 1989.

Showman, A. P. and R. Malhotra, Tidal evolution into the Laplace resonance and the resurfacing of Ganymede, *Icarus* **127**, 93–111, 1997.

Showman, A. P., D. J. Stevenson, and R. Malhotra, Coupled orbital and thermal evolution of Ganymede, *Icarus* **129**, 367–383, 1997.

Smith, B. A., L. Soderblom, R. F. Beebe, J. M. Boyce, G. Briggs, A. Bunker, S. A. Collins, T. V. Hansen, C.and Johnson, J. L. Mitchell, R. J. Terrile, M. H. Carr, A. F. Cook, J. N. Cuzzi, J. B. Pollack, G. E. Danielson, A. P. Ingersoll, M. E. Davies, G. E. Hunt, H. Masursky, E. M. Shoemaker, D. Morrison, T. Owen, C. Sagan, J. Veverka, R. Strom, and V. E. Suomi, Encounter with Saturn: *Voyager 1* imaging science results, *Science* **212**, 163–191, 1981.

Squyres, S. W., Topographic domes on Ganymede: Ice vulcanism or isostatic upwarping, *Icarus* **44**, 472–480, 1980.

Stewart, S. T., T. J. Ahrens, and J. D. O'Keefe, Large martian regolith water content implied by rampart crater population, in *Eos*, p. F726, 2001.

Strom, R. G., A. Woronow, and M. Gurnis, Crater populations on Ganymede and Callisto, *J. Geophys. Res.* **86**, 8659–8674, 1981.

Tabe, I., J. Watanabe, and M. Jimbo, Discovery of a possible impact spot on Jupiter recorded in 1690, *PASJ* **49**, L1–L5, 1997.

Thomas, P. J. and G. Schubert, Power law rheology of ice and the relaxation style and retention of craters on Ganymede, *J. Geophys. Res.* **93**, 13 755–13 762, 1988.

Thomas, P. J. and S. W. Squyres, Formation of crater palimpsests on Ganymede, *J. Geophys. Res.* **95**, 19 161–19 174, 1990.

Trujillo, C. A., D. C. Jewitt, and J. X. Luu, Properties of the Trans-Neptunian Belt: Statistics from the Canada-France-Hawaii Telescope Survey, *AJ* **122**, 457–473, 2001.

Turtle, E. P. and B. A. Ivanov, Numerical simulations of impact crater excavation and collapse on Europa: Implications for ice thickness, in *Lunar and Planetary Science Conference Abstracts*, p. 1431, 2002.

Turtle, E. P. and E. Pierazzo, Thickness of a Europan ice shell from impact crater simulations, *Science* **294**, 1326–1328, 2001.

Wagner, R., U. Wolf, G. Neukum, and the *Galileo* SSI Team, Ages of individual craters on the Galilean satellites Ganymede and Callisto, in *Lunar and Planetary Science Conference Abstracts*, p. 1818, 1999.

Weaver, H. A. and P. L. Lamy, Estimating the size of Hale–Bopp's nucleus, *Earth, Moon and Planets* **79**, 17–33, 1999.

Williams, K. K. and M. T. Zuber, Measurement and analysis of lunar basin depths from *Clementine* altimetry, *Icarus* **131**, 107–122, 1998.

Woronow, A., R. G. Strom, and M. Gurnis, Interpreting the cratering record: Mercury to Ganymede and Callisto, in *Satellites of Jupiter*, D. Morrison (ed), University of Arizona Press, pp. 237–276, 1982.

Zahnle, K., L. Dones, and H. F. Levison, Cratering rates on the Galilean satellites, *Icarus* **136**, 202–222, 1998.

Zahnle, K., P. Schenk, S. Sobieszczyk, L. Dones, and H. F. Levison, Differential cratering of synchronously rotating satellites by ecliptic comets, *Icarus* **153**, 111–129, 2001.

Zahnle, K., P. Schenk, H. Levison, and L. Dones, Cratering rates in the outer solar system, *Icarus* **163**, 263–289, 2003.

Zimmer, C., K. K. Khurana, and M. G. Kivelson, Subsurface oceans on Europa and Callisto: Constraints from *Galileo* magnetometer observations, *Icarus* **147**, 329–347, 2000.